Prognostics of Power Electronic Converters in Renewable Energy Systems: An Approach Based on Acoustic Emission Measurement and Thermal Modelling

P BOLOURINEJAD

PhD   2024

Prognostics of Power Electronic Converters in Renewable Energy Systems: An Approach Based on Acoustic Emission Measurement and Thermal Modelling

Pouria Bolourinejad

Abstract

Renewable energy conversion systems play an important role in delivering energy from natural resources. Power Electronic Converters (PECs) are vital for efficiently conditioning the generated energy to align with the requirements of the source. One of the obstacles in the wide adaptation of renewable energies is the lack of efficiency and reliability in these systems. In wind turbines, Electrical circuits, including the PEC, contribute to 24% of total failures experienced by the system. One of the key components in a PEC is the Insulated Gate Bipolar Transistor (IGBT) which is used as a switching device in PECs. They occur due to different factors such as operating conditions, environmental factors (temperature and humidity) and the internal structure of the IGBTs which are formed of layers of different material with different properties.

This research focuses on exploring the relationship between the changes in temperature of the IGBT chip with acoustic emissions signals. The aim of this research project is the development of a more cost-effective method for condition monitoring and prognostics of PECs.

In this thesis, a thorough literature review of current condition monitoring schemes is provided and the gap in research is identified. A great number of scholars and experts have experimented with the AE in PECs however the link between the increase in temperature of this chip and the fluctuations in AE signals is not yet established. Under certain loading conditions, the temperature of IGBT chip changed from the ambient temperature ($20°C$) to $55°C$. The acoustic emissions were measured in $5°C$ intervals and it was discovered that after the temperature surpasses the $40°C$ mark, the AE signal amplitude drops to 0.1 percent of its value at $20°C$. Moreover, the rising temperature creates new peaks in the frequency domain at frequencies between 400-600 kHz.

Declaration

No portion of the work referred in this thesis has been submitted in support of an application for another degree or qualification at this, or any other university, or institute of learning.

Acknowledgement

I would like to express my profound gratitude to everyone who supported me throughout the course of this PhD journey.

First and foremost, I wish to express my heartfelt thanks to my Director of Studies, Prof. Albarbar, whose expertise, understanding, and patience added considerably to my doctoral experience. His continued encouragement and insightful critiques throughout this process made this accomplishment possible.

I am deeply indebted to my advisory committee member, Dr Canras Batunlu, for his unwavering support, invaluable guidance, and constructive criticism during the initial, crucial stages of this project. His expertise and intelligent suggestions have been vital for the progress of my research.

To my dear parents, Noushin and Ahmad, words cannot express my gratitude for your love, prayers, and endless support throughout my life. This achievement would not have been possible without your unwavering faith in my capabilities and your constant encouragement. Thank you for being my first and greatest teacher.

I would also like to sincerely appreciate my partner, Karishma. Your constant support, patience and love were my beacon during the challenges I faced throughout this journey. Your belief in my abilities provided the strength I needed to persevere.

Lastly, to my sister and brother-in-law, Pantea and Pejman, I want to express my heartfelt gratitude. Your continued moral support and faith in me provided a boost whenever I felt overwhelmed.

To all of you, I dedicate the fruit of this effort. Thank you.

Table of Contents

Table of Figures

List of Tables

List of Abbreviations

2L-BTBC	Two Level Back to Back Converter
3L-NPCC	Three Level Neutral Point Clamped Converter
AE	Acoustic Emissions
DC	Direct Current
FEM	Finite Element Model
FFT	Fast Fourier Transform
IGBT	Insulated Gate Bipolar Transistor
IGCT	Integrated Gate-Commutated Thyristor
PEC	Power Electronic Converter
PWM	Pulse Width Modulation
RECS	Renewable Energy Conversion Systems

Chapter 1 : Introduction and Background

1.1 Motivation

In recent years, the importance of renewable energy sources has become increasingly evident as they are the key to foster long term environmental and economic sustainability. Renewable energy conversion systems (RECS) convert the energy from natural sources such as wind, solar, hydro, geothermal and biomass to electricity. Power electronic converters (PECs) play a vital part in controlling and conditioning the generated electricity from RECSs. This thesis focuses on the PECs used in wind turbine systems.

A wind turbine consists of multiple subsystems, each experiencing failures at varying rates throughout its lifespan and under different operational modes and loading conditions.
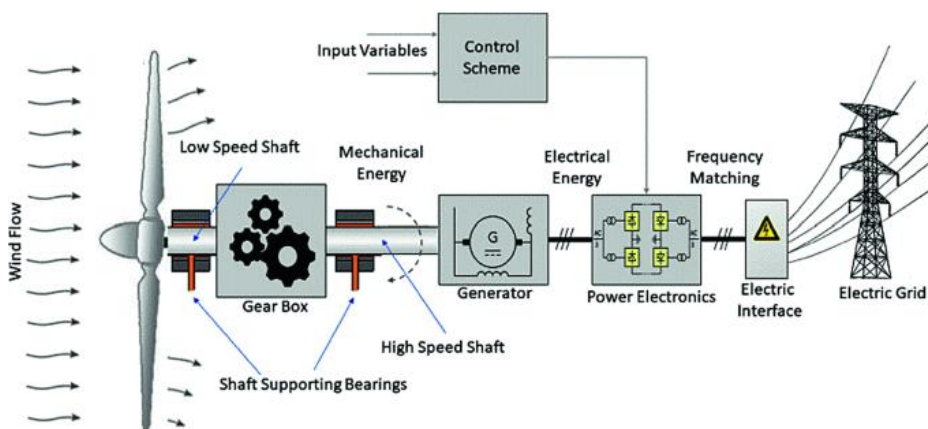
Figure 1-1. Components in a wind turbine hub (Ganthia et al., 2021)

The wind turbine's blades are designed to capture the kinetic energy of the wind. These blades rotate when exposed to the wind. The rotating blades are connected to a rotor shaft. As the blades turn, they spin the rotor shaft. The rotor shaft is connected to a generator through a gearbox. As the rotor shaft spins, it rotates the generator's rotor, which is surrounded by a

stationary set of coils. This relative motion induces an electric current in the coils through electromagnetic induction generating electricity. The generated power is then passed through the Power Electronic Devices to condition the signal. This is required to match the characteristics of the generated electricity with the requirements of the grid.

Li et al. (2022) analysed the reason for failures in a sample of wind turbines. It was established that the cooling & hydraulic system is the leading cause of failure in wind turbines. The second highest failure rate is registered for electrical facilities, which includes the PECs. One of the crucial components in PECs is the power transistor. Insulated-gate bipolar transistors (IGBT) are widely used in PECs. Power semiconductors in PECs are driven by frequencies of between 20-50 kHz. The constant switching of these devices in high frequencies leads to thermos-mechanical stress and exposes the device to long periods of high temperature which ultimately results in the failure of IGBTs.
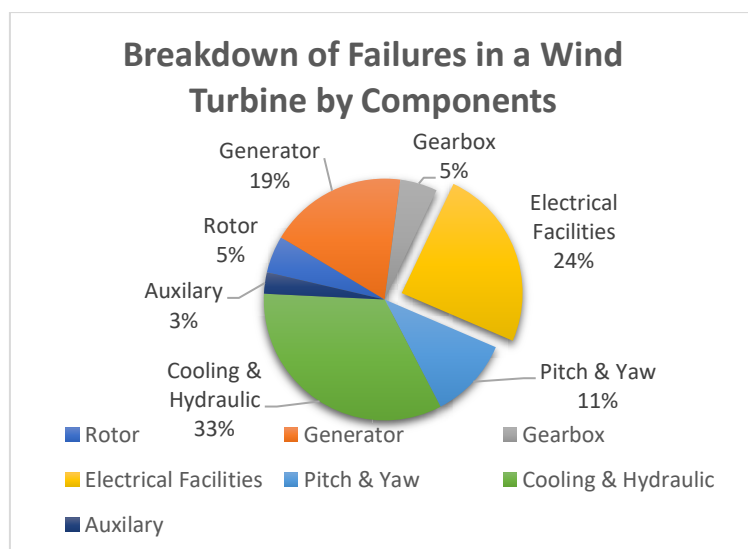
Figure 1-2 Number of failure modes in wind turbines (Li et al., 2022)

Failure in a wind turbine results in financial penalties and reduced delivery of electricity. As a result, it's essential to design and implement robust condition monitoring techniques to identify failures in time before a failure occurs. This leads to lower downtime in a wind turbine and maximum efficiency.

1.2 Power Electronic Converters

PECs play a crucial part in the integration and efficient utilisation of renewable energy systems. They are responsible for transforming and controlling the energy generated by renewable energy sources such as wind turbines and solar panels. By utilising PECs, the variable and often unpredictable nature of renewable energy sources can be managed and optimised. They enable the integration of renewable energy systems into the existing power infrastructure. Therefore, the role of PECs is pivotal in promoting the widespread adoption and successful integration of renewable energy systems into the modern power grid.

Three types of PECs are used in RECSs: buck, boost and buck-boost converters.

1.2.1 Buck Converters

A buck converter, also known as a step-down converter, is a DC-DC power converter that converts higher voltage levels to lower ones while maintaining a stable output voltage. Buck converters utilise a power semiconductor such as an IGBT that switches on and off in high frequencies. This power semiconductor is usually controlled by a pulse-width modulation (PWM)

signal. When the switch is on, current flows through an inductor, storing energy in its magnetic field. When the switch is off, the inductor releases its' stored energy to the load (Castaldo, 2012).
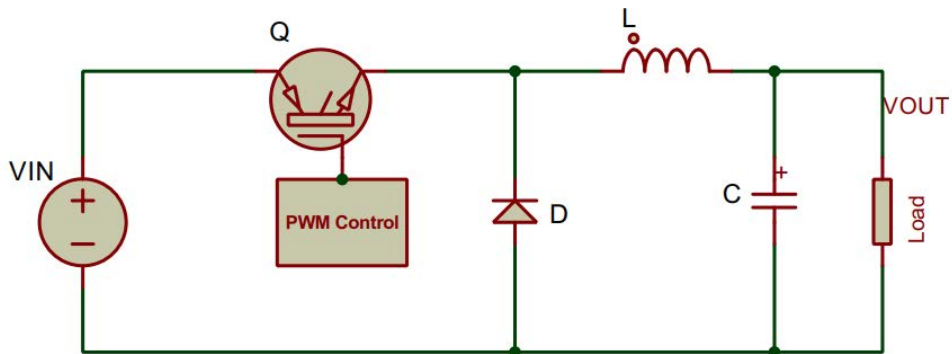
Figure 1-3. Buck Converter circuit diagram(Castaldo, 2012)

1.2.2 Boost Converter

The boost converter is also known as a step-up converter. It's a DC-DC converter that increases a lower DC input voltage to a higher DC output voltage.

Initially, when the power switch is closed, current flows through the inductor and increases at a rate determined by the input voltage. The inductor stores energy in its magnetic field. When the switch is opened, it causes the current to drop to zero. The inductor then releases the stored energy trying to maintain the current flow. The increased voltage across the inductor causes the diode to go into forward-biased mode and start conducting. It allows the inductor's stored energy to flow through the diode and charge the output capacitor. The output capacitor is then charged, and its voltage increases, providing a higher output voltage than the input voltage. The output voltage

can be controlled by adjusting the PWM duty cycle (D), which is the ratio of switch-on time to the total switching period.

Boost converters are commonly used in applications such as battery-powered devices and renewable energy systems. (Castaldo, 2012) Figure 1.4 demonstrates the circuit diagram for a boost converter used in a wind turbine.
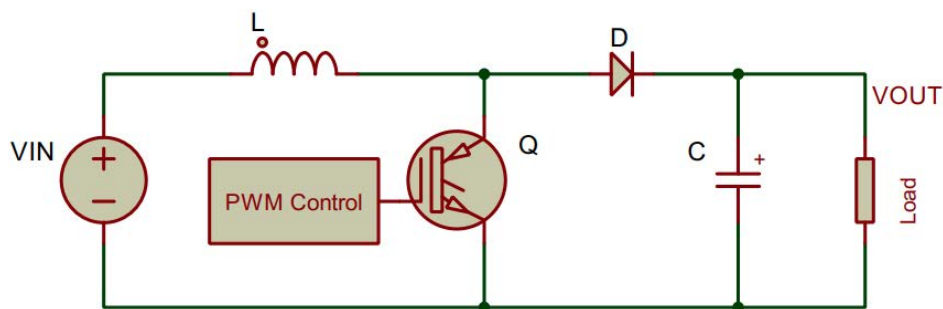
Figure 1-4. Boost converter circuit diagram (Castaldo, 2012)

1.2.3 Buck-Boost Converters

A buck-boost converter is a DC-DC power converter that can step up or down the input voltage to provide the desired output voltage level. It is a combination of boost and buck converters in a single circuit.

During the buck mode (step-down), the power switch is closed, allowing the current to flow through the inductor. The inductor stores energy in its magnetic field and the output voltage is lower than the input voltage. During the boost mode (step-up), the power switch is opened, leading to a drop in the current. Due to the reverse polarity, the diode becomes reverse-biased. The output voltage is now higher than the input voltage. (Castaldo, 2012)
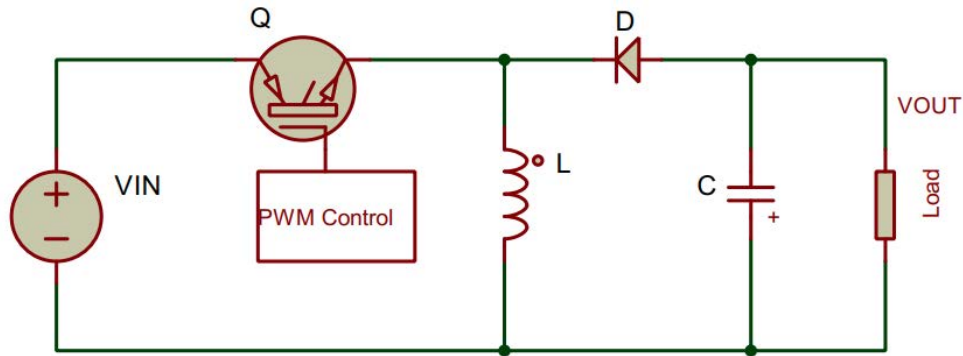
Figure 1-5. Buck-boost converter circuit diagram (Castaldo, 2012)

In this research, the focus is on the boost converters used in wind turbines.
The outcome of this research is expandable to any PECs that have a power
semiconductor, an IGBT in this case. The power semiconductor used in these
PECs have similar degradation and failure mechanisms, and by studying one
of the above circuits, boost converter in this case, in a specific RECS, a wind
turbine in this study, the results can be applied to a wide range of PECs used
in a variety of RECSs.

1.3 Failure Mechanism of Power Semiconductors

In PECs, stresses are imposed by factors such as environmental conditions,
electrical loading and mechanical vibrations.

Chip-Related Failure Mechanisms	Packaging-Related Failure Mechanisms
Electrical Overstress	Bond Wire Lift Off
Electrical Discharge	Solder Fatigue
Latch-Up and Triggering of Parasitic Charge Effect	Electrical Stress Effects
Electromigration, Contact and Stress-Induced Migration External Radiation	

Table 1. Failure Mechanism in Power Electronic Devices (Yang et al., 2010)

The failure mechanisms for PECs are categorised into two groups, chip-related and packaging-related (Yang et al., 2010). Table 1 categorises these failure modes into two distinct groups of chip-related and packaging-related failure mechanisms.

Potential Failure Modes	Potential Failure Causes	Parameters affected
Short circuit, loss of gate control, increased leakage current (Oxide)	High temperature, high electric field, overvoltage	Time dependent dielectric breakdown (V_{th}, g_m)
Loss of gate control, device burn-out (Silicon die)	High electric field, overvoltage, ionising radiation	Latch-up ($V_{CE(ON)}$)
High leakage currents (Oxide, Oxide/Substrate Interface)	Overvoltage, high current densities	Hot electrons (V_{th}, g_m)
Open Circuit (Bond Wire)	High temperature, high current densities	Bond Wire Cracking, Lift Off ($V_{CE(ON)}$)
Open Circuit (Die Attach)	High temperature, high current densities	Voiding, Delamination of Die Attach ($V_{CE(ON)}$)

Table 2. Failure Mechanism in Power Electronic Converters (Valentine et al., 2015)

Valentine et al. (2015) categorised these failure mechanisms into three top-level categories, short circuit, open circuit and parameter drift. A summary of these failure modes and mechanisms is demonstrated in Table 2.

1.4 Condition monitoring

Condition monitoring (CM) is a technique or process of monitoring specific parameters in a system so that any fluctuations in the monitored parameter will alert the user to schedule maintenance. Condition monitoring aims to identify any abnormalities in the early stages to avoid total system failure. There are three different processes in detecting faults:

1. Diagnosis: Finding the root cause when a failure occurs in a system

2. Prognosis: Monitoring the current health of the system and predict the health of the components in the system, providing a prediction of health of these components in the future.

3. Condition Monitoring: Constantly monitoring the system in real time so if any abnormalities is observed, an action is needed to be taken. (Yang et al., 2010)
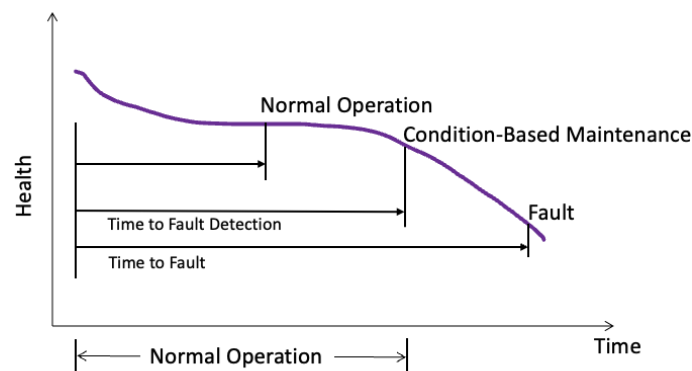
Figure 1-6. Overview of Diagnosis, Prognosis and Condition Monitoring Schemes (Yang et al., 2010)

A review of the most recent CM schemes used in PECs are thoroughly discussed in Chapter 2. For the purpose of this research, electrothermal stress and acoustic emissions (AE) are studied.

1.4.1 Thermomechanical Stress

One of the most common modes of failure in PECs is the thermomechanical fatigue experienced by the power semiconductor. In PECs, the thermal modelling of power semiconductors assists the manufacturers in identifying areas of heat dissipation. As demonstrated in Figure 1.7, an IGBT chip consists of different layers with unique material properties. During the operation of an IGBT, heat is transferred through these different layers. As a result, thermal stress occurs within these materials due to different coefficients of thermal expansion (CTE). (Yang et al., 2010) The properties of each material in an IGBT chip are detailed in Table 5 of Chapter 3. This ranges from 2.6 ($10^{-6}K^{-1}$) for Silicon to 23.5 ($10^{-6}K^{-1}$) for Aluminium.
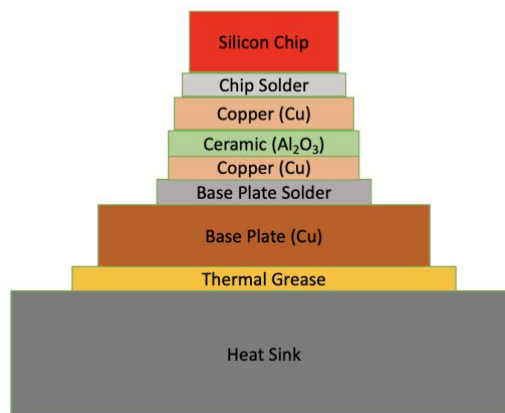
Figure 1-7. The internal structure of an IGBT chip

1.4.2 Acoustic Emissions (AE)

In condition monitoring PECs, acoustic emissions is defined as the emission of vibrations (Karkkainen et al., 2014). The power semiconductor used in PEC is driven by a pulse width modulated signal (PWM) with a frequency of between 20-50 kHz. This indicates that the power semiconductor, IGBT in

this case switches between on and off states tens of thousands of times in a second. This constant switching produces acoustic emissions which can be captured by AE sensors and an AE data acquisition system. The constant switching of the power semiconductor also dissipates heat. Variations in the junction temperature (T_j) cause constant thermomechanical stresses in the power semiconductor module affecting the generation of AE signals. Acoustic emissions in PECs can provide valuable information on the operational state of the converter and they can aid in fault detection, performance assessment and predictive maintenance. Researchers from different academic institutions have invested in the thermal characteristics of the IGBT chip under operation. However, the link between the acoustic emissions and the thermal behaviour of the IGBT chip is not established yet. AE monitoring enables renewable energy site owners and manufacturers to design a remote, robust and non-intrusive condition monitoring scheme. The power semiconductor is the only device in a PEC that emits the AE and therefore there is no interference. Whereas for the thermal monitoring, the temperature is impacted by the surrounding components.

1.5 Aim and Objectives:

The aim of this research project is the design and implementation of a real-time condition monitoring scheme for power electronic converters used with solar, wind and fuel cell energy systems. It is intended to make use of non-intrusive condition monitoring techniques such as acoustics and thermal to

detect any failures, at early stages of their occurrence, identify causes of such failures and estimate their remaining life.

1.5.1 Objectives

1. Gain a clear understanding of the characteristics and working principles of power electronic devices with a focus on those used with renewable energy systems. Namely, boost converters, buck converters, rectifiers and inverters used with solar, wind and fuel cell systems.

2. Literature review of the common failure modes of power electronic devices (PEDs) and currently used monitoring techniques.

3. Develop an Insulated Bipolar Gate Transistor (IGBT) thermal model in COMSOL to understand the effect of thermal stress on the failure modes and the influence of such stresses on AE generation and propagation

4. Verify the outcomes of the developed models through a purposely-designed experimental setup. Measurements of temperature and acoustic emissions in addition to power parameters are expected to be recorded under different operating conditions.

1.6 Publications and Presentations

1. Badawood, A., Alrweg, M., Musaad, H., Bolourinejad, P., Albarbar, A. and Batunlu, C. (2017) 'Acoustic Emission Based Condition Monitoring Technique for Power Electronic Devices used in Solar

Power Systems'. In: World Congress on Condition Monitoring. London: The British Institute of Non-Destructive Testing. (Publication)

2. Bolourinejad, P. 'Model-Based Approach to Condition Monitoring for Power Electronic Devices Inside Renewable Energy Conversion Systems' In: MMU Science Symposium. Manchester, Manchester Metropolitan University (Poster Presentation)

1.7 Structure of the Remaining Chapters

This thesis is outlined in 6 chapters as follows:

Chapter 2 focuses on a literature review of current health management and condition monitoring methods. In this chapter, different modes of failure in PEC are explained. Moreover, different topologies that the PECs are used are covered outlining the advantages and disadvantages of each topology. Lastly, the gap in research is identified and the importance of utilising AE as a condition-monitoring tool is highlighted.

Chapter 3 explains the process of designing a FEM of the IGBT chip. The reasons for electrothermal and thermomechanical stresses exerted on the device is explained. It is followed by the simulation of the IGBT chip in the same operating condition as the experimental circuit.

Chapter 4 covers the instrumentation required for the measurement of AE signal from the IGBT chip in a boost converter circuit. The result of the experiment is presented in this chapter alongside a brief discussion of the results.

Chapter 5 focuses on the interpretation of the measured AE signal in time domain and frequency domain. The results and findings are discussed and the relationship between changes in IGBT temperature and the level of acoustic emissions is shown.

Chapter 6 summarises the research and findings and how the objectives of this research are achieved. Moreover, the future work for this project is outlined.

Chapter 2 : Literature Review and Identification of the Research Gap

2.1. Introduction

This chapter presents a literature review on the condition monitoring of PECs used in RECSs. First, different failure modes due to electrothermal stress is discussed. Furthermore, the recent condition monitoring schemes used in PECs is reviewed. Lastly, the gap in the research is identified and the main direction for this research is outlined.

2.2 Power Electronic Converters

Power electronics pertains to the utilisation of static methods for effectively converting, controlling, and conditioning electric power to achieve the desired output form. Power electronic circuits encompass a broad range of electric energy conversions, covering power levels spanning from tens of watts to hundreds of megawatts. This wide power range is evident in the diverse overall sizes of PE setups. While some arrangements can fit in the palm of a hand, others necessitate dedicated spaces specifically designed for their operation.(Strzelecki and Zinoviev, 2008).

The PEC used in a wind turbine serves as the intermediary between the wind turbine generator and the power grid. It needs to meet the requirements of both sides. Regarding the generator side, it is necessary to control the current in the generator stator to regulate torque, thereby influencing the rotational speed. This control is crucial for maintaining active power balance during normal operation, enabling the extraction of maximum power from the wind turbine, and also in scenarios where grid faults occur (Hansen and Hansen, 2007). Additionally, the converter should possess the capability to

handle the variable fundamental frequency and voltage amplitude of the generator output in order to control the speed. On the grid side, the wind power converter must adhere to the grid codes irrespective of the wind speed. This entails having the capability to regulate the inductive or capacitive reactive power (Q) and respond quickly to changes in active power (P). Under normal operation, the converter should maintain a relatively constant fundamental frequency and voltage amplitude on the grid side. Additionally, it is essential to keep the total harmonic distortion (THD) of the current at a low level. (Timbus et al., 2005)

The advancement of switching devices is playing a significant role in enhancing the reliability and efficiency of higher power converters utilised in wind turbines. Key choices in this field include IGBT modules, IGBT press packs, and IGCT press packs.(Blaabjerg et al., 2012)

In comparison to power modules, press-pack IGCT offers advantages such as higher power density allowing easier stacking for series connection, and improved cooling capability. However, these benefits come at a higher cost. While press-pack IGCT technology supports the advancement of medium voltage (MV) converters and is already considered state-of-the-art in high-power electric drives for applications like oil and gas, its adoption in the wind turbine industry is not yet widespread, partially due to cost considerations. (Jakob et al., 2007; Alvarez et al., 2011; Busca et al., 2011). A comparison between the 3 different technologies is demonstrated in Table 3.

	IGBT	IGBT Press-pack	IGCT Press-pack
Power Density	Moderate	High	High
Reliability	Moderate	High	High
Cost	Moderate	High	High
Failure Mode	Open Circuit	Short Circuit	Short Circuit
Thermal Resistance	Moderate	Small	Small
Switching Loss	Low	Low	High

Table 3. Main Switching Devices for Wind Power Converters

The PECs are designed either as a single-cell, two-level or multilevel systems for wind turbines. In the next section the operation, advantages and disadvantages of these converters are discussed.

2.2.1 Single-Cell Power Electronic Converters

Several wind turbine manufacturers, use a permanent magnet synchronous generator (PMSG) in a full-rated power converter wind turbine. Since the generator in this scenario does not require reactive power and the active power flows unidirectionally from the (PMSG) to the grid through a power converter, a cost-effective solution can be achieved by using a simple diode rectifier for the generator side converter. However, it's important to note that even if the diode rectifier is multiphase or 12-pulses, it can introduce low-frequency pulsations that have the potential to trigger shaft resonance. (Faulstich et al., 2005) To achieve variable speed operation and maintain a stable DC bus voltage, there are two options: incorporating a boost DC-DC

converter in the DC link or controlling the DC voltage through rotor excitation, as demonstrated in Figure 2.1. It is important to note that for power levels in the megawatt range, the DC/DC converter needs to be constructed using multiple interleaved units or a three-level solution.(Wu et al., 2005)
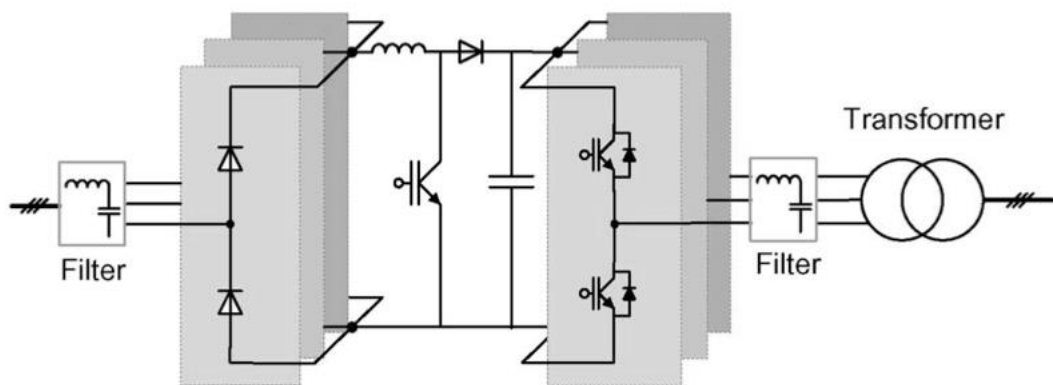
Figure 2-1. Full-rated power electronic converter circuit in a wind turbine with PMSG (Blaabjerg et al., 2012)

Figure 2.2 demonstrates the use of two current source converters in a back-to-back connection. One potential benefit of the suggested solution is the utilisation of the inductance offered by the lengthy cables employed in wind parks, especially when a DC distribution system is implemented. This advantage can also be applied in scenarios where the generator converter is positioned in the nacelle while the grid converter is situated at the base of the wind turbine system (WTS). (Tenca et al., 2008)
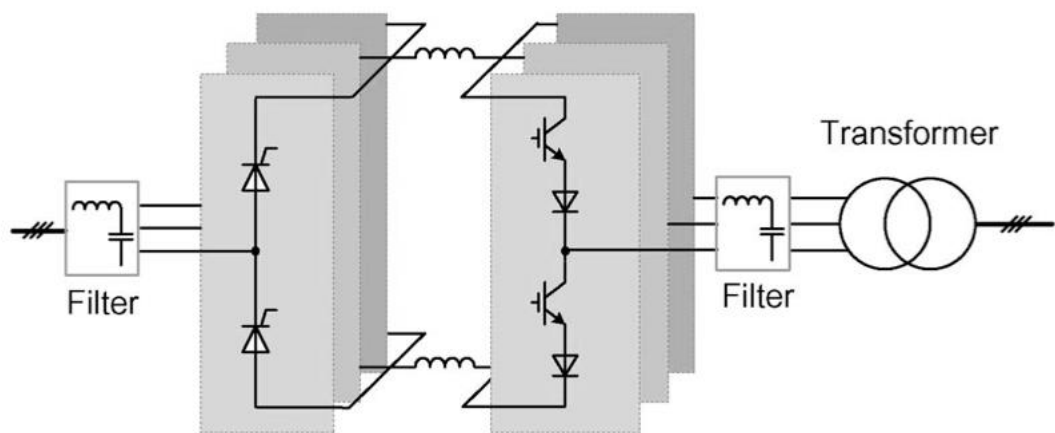
Figure 2-2. Full-rated power converter wind turbine with PMSG with two current sources (Blaabjerg et al., 2012)

2.2.2 Two-Level Power Converter (2L-BTB)

The most commonly used three-phase power converter topology in wind turbine systems is the Pulse Width Modulation-Voltage Source Converter with a two-level output voltage (2L-PWM-VSC). Another widely utilised topology is the two-level back-to-back voltage source converter (2L-BTB). As the PEC used in wind turbines, two 2L-PWM-VSCs are usually set up as a back-to-back structure with a transformer on the grid side as seen in Figure 2.3. (Blaabjerg et al., 2012). The advantage of this topology is the simple structure and fewer components which is the reason it is known to have a robust and reliable performance. One disadvantage associated with this model is by increasing the voltage range of the wind turbine, this configuration suffers from larger switching losses and lower efficiency at MW power levels.
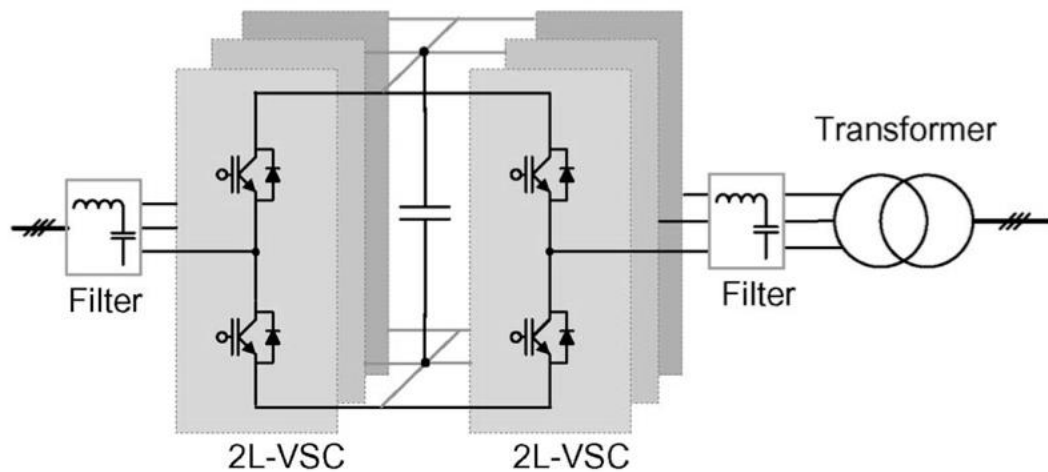
Figure 2-3. Two-Level back-to-back voltage source converter for wind turbines (2L-BTB)(Blaabjerg et al., 2012)

2.2.3 Multilevel Power Converter

With the increasing power capacity of wind turbines, reaching up to 10 MW, it has become progressively challenging for conventional two-level back-to-back (2L-BTB) solutions to achieve satisfactory performance using the currently available power semiconductors multilevel converter topologies are gaining interest and popularity in wind turbine applications due to their capabilities of offering more output voltage levels, higher voltage amplitudes, and greater output power. Multilevel converters can be categorised into three main groups; neutral point diode clamped structure, flying capacitor clamped structure, and cascaded converter cells structure. (Teichmann and Bernet, 2005; Carrasco et al., 2006; Rodriguez et al., 2010) There are a variety of multilevel PECs topologies commercially used in wind turbines.

- Three-Level Neutral-Point Diode Clamped Back-To-Back (3L-NPC BTB)

- Three-Level H-Bridge Back-to-Back (3L-HB BTB)

- Five-Level H-Bridge Back-to-Back (5L-HB BTB)

- Three-Level Neutral-Point Diode Clamped (3L-NPC + 5L-HB)

	3L-NPC	3LHB	5L-HB	3L -NPC + 5L-HB
Number of IGBTs	24	24	48	36
Diode Numbers	36	24	72	54
Advantages	Matured technology	Less DC link capacitors, Equal loss distribution	More output voltage levels, higher voltage utilisation of device	Higher performance on grid side than generator side
Disadvantages	Unequal loss distribution	More cables required	More cables and devices required	Unequal loss distribution

Table 4. Comparison of different multilayer PEC topologies(Blaabjerg et al., 2012)

Each of the above offers advantages and disadvantages when used for different applications. Table 4 summarises the characteristics of each of the above topologies while comparing their advantages and disadvantages.

Various topologies for PECs used in wind turbines were discussed above. Depending on the wind turbine's application and size, a different topology is utilised to convert the generated power to a magnitude and frequency accepted by the grid code. The use of an IGBT chip as the power semiconductor is common in all the above topologies. The outcome of this PhD research applies to all the above topologies as they all use a power semiconductor as the switching device in their circuit.

2.3 Failure Modes in Power Electronic Converters

When a PEC is utilised in various applications, the converter's components are susceptible to failures caused by temperature fluctuations, humidity and moisture, contaminants, dust, and vibrations. In Chapter 1, it was demonstrated that PECs are accountable for 21% of failures in a wind turbine system. Figure 2.4 reflects the percentage of each of the above environmental factors in the failure of an IGBT.
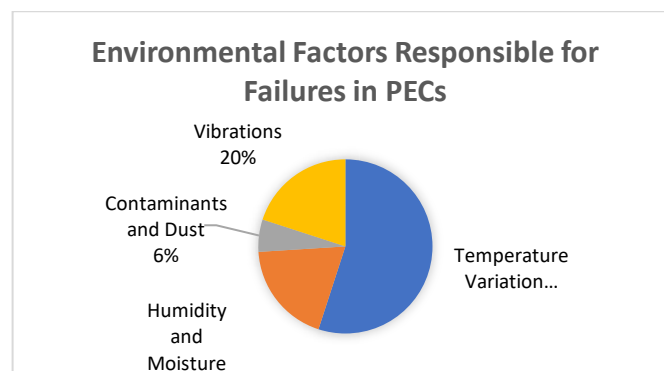
Figure 2-4. Environmental factors responsible for failures in PECs (Meher et al., 2021)

As discussed in Chapter 1, failure modes in an IGBT chip can be categorised into chip-related and package-related failures.

2.3.1 Chip-Related Failure Mechanisms

Failure mechanisms related to chips are essentially responsible for the destruction of a device. These mechanisms are distinct from packaging-related issues but can be interconnected during a failure event. Commonly acknowledged factors such as overstress and wear-out mechanisms during operation are believed to induce specific deteriorations and potential failures over the long term. It is crucial to give serious consideration to these factors when implementing a condition monitoring scheme and designing a converter. (Amerasekera and Njim, 1997; Ohring and Kaszprzak, 2014)

2.3.1.1 Electrical Overstress (EOS)

Electrical overstress (EOS) arises from excessive voltage or current conditions. The presence of high voltages can lead to significant heating effects, and the risk of secondary breakdown becomes a major concern for certain devices. It is imperative to ensure that the power device's Safe Operating Area (SOA) is appropriate for the application and that the heat sinking specification for the component is met. (Amerasekera and Njim, 1997) In the case of thyristors, nonuniform current distribution during turn-off caused by rapid di/dt can result in increased power dissipation and eventual thermal damage. Furthermore, a rapidly rising voltage ramp can induce displacement current, triggering unintended device turn-on potentially leading to short circuits and failures. (Sze, 1981)

2.3.1.2 Electrostatic Discharge (ESD)

Electrostatic Discharge events can cause partial puncturing of the gate oxide, leading to the device initially functioning adequately and passing inspection. However, over time, this can result in device failure. Gate shorting has been observed as a consequence of ESD, particularly when the gate is subjected to excessive voltage without any protective measures in place. The detection of partial gate failure can be achieved by measuring the decay time constant of the gate charge.(Grant and Gowar, 1989)

2.3.1.3 Latch-Up and Triggering of Parasitics

Large values of dv/dt during turn-off may result in triggering of the parasitic thyristor in IGBTS. The capacity of a device to handle energy can vary depending on the location of the failure [37]. While latch-free technology has been developed (Baliga, 1995), it is crucial to implement appropriate circuit design to limit the ramp rate of reapplied voltage within the reverse bias Safe Operating Area (SOA) to prevent latch-up (Kameda, 2008).

2.3.1.4 Charge Effect

Charge effect failure modes are common in metal-oxide-semiconductor field-effect transistors (MOSFET). The charge effect failures have two subcategories; The first involves the distortion of the electric field due to the accumulation of ionic contaminants in the passivation layer of the high-field region. The second mechanism involves the development of defects in the gate oxide (Grant and Gowar, 1989). These two mechanisms result in fluctuations in the performance characteristics of the device, including the

threshold voltage, leakage current, transconductance, and saturation current. Over time, these shifts in performance can lead to the degradation of the device.(Maouad et al., 2000; Patil et al., 2008)

2.3.1.5 Thermal Activation

The increase in temperature amplifies thermally activated processes, as outlined by Arrhenius' law.

$$rate\ of\ activation\ \propto \exp{(-\frac{E_a}{RT})} \qquad (1)$$

Where:

E_a : Activation Energy (J/mole)

T: Temperature (Kelvin)

R: Gas constant (J/mole.kelvin)

The increased temperature accelerates the degradation process for almost all silicon-based power devices. (Grant and Gowar, 1989)

2.3.2 Package-Related Failure Mechanisms

The most commonly observed failure mechanisms in power electronic devices are the thermomechanical fatigue stress endured by the packaging materials.(Ciprian et al., 2009) The primary factors leading to these failure mechanisms are the disparities in the coefficients of thermal expansion (CTE) among the various materials in the chip and package, along with the localised temperature fluctuations they experience.(Ciappa et al., 2007)
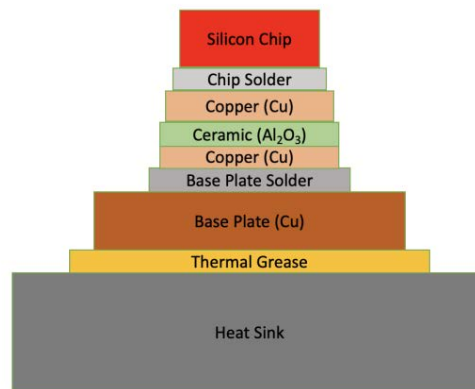
Figure 2-5. The internal structure of an IGBT chip

The internal structure inside an IGBT chip consists of different layers made with different materials. The packaging-related failure modes are mostly because of the difference in the coefficient of thermal expansion (CTE) between these layers as seen in Figure 2.5. Three types of packaging-related failure modes in IGBTs are addressed below.

2.3.2.1 Bond Wire Lift-off

Bond wire lift-off primarily occurs due to crack growth at the interface between the bond wire and the chip. It is triggered by temperature fluctuations and the different CTEs between silicon (Si) and aluminium (Al). (Held et al., 1997) The dissimilarity in strain between the two materials induces stress at their interface, and temperature variations influence this stress. The initiation and progression of cracks are then driven by the energy loss associated with stress-strain hysteresis as the temperature, and consequently, the stress undergoes cyclic changes during operation. (Yang et al., 2010) Figure 2.6 demonstrates a typical crack propagation in a wire bond. During thermal fatigue testing, when there are significant temperature

swings (ΔTj) at the junction, cracks tend to propagate from both ends towards the centre along the fine grain boundaries of the aluminium (Al) wires. Once the crack reaches the centre, the bond wire becomes detached or lifts off. (Held et al., 1997)
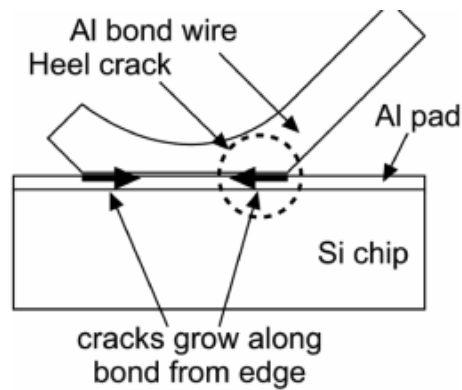
Figure 2-6. Bond wire lift-off due to crack growth

2.3.2.2 Solder Fatigue

Solder fatigue and cracking between the power module substrate and the base plate, as well as between the device chip and substrate, are significant failure modes observed in power modules. (Ratchev et al., 2004) Solder failures can be attributed to factors such as the initial microstructure of the solder, metallisation of the substrate, and the presence of intermetallic compounds.(Thebaud et al., 2000) this failure occurs due to the difference in the CTE between the silicon die and copper substrate, leading to shear stress within the solder layer and ultimately causing crack formation as shown in Figure 2.7. This will limit the area for heat to transfer from the die and it leads to rising temperature on the die. The localised hot temperature due to the increased thermal resistance of the die attach leads to damage to the chip.(Katsis and van Wyk, 2003)
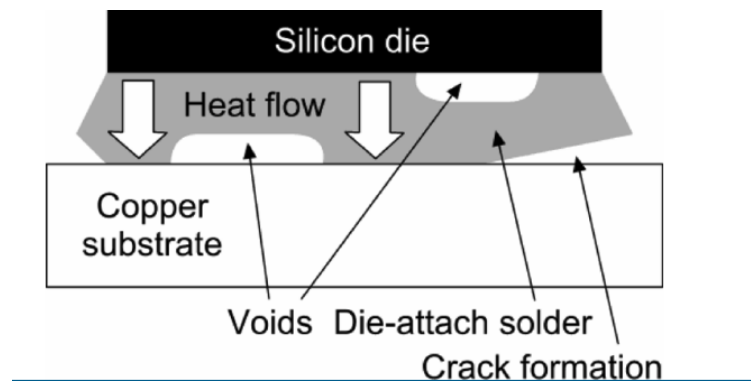
Figure 2-7.Crack growth in die-attach solder (Yun et al., 2001)

2.3.2.3 Electrical Stress Effect

(Han and Song, 2003)expansion. This research demonstrated that the on-state I-V curves of IGBTs are dependent on applied stress. It showed a 10% change in the on-state voltage resulting from shear stress on the device chip.

2.4 Condition monitoring

Condition monitoring (CM) refers to the practice of monitoring the operational behaviour of a physical system to detect any changes in its characteristics. This enables the scheduling of maintenance activities before significant deterioration or failure takes place. CM involves regularly observing and analysing the monitored characteristics to identify any deviations from normal operating conditions, allowing for timely intervention and preventive actions. By proactively addressing potential issues, CM aims to enhance system reliability, minimise downtime, and optimise maintenance strategies. In this section, a literature review of current condition monitoring systems is discussed and the gap in research is identified. The main methods of condition monitoring PECs are categorised

into three sections, thermal modelling-based CM, acoustic emissions-based

CM and electrical parameter based CM

2.4.1 Thermal Modelling

Thermal models are created to analyse the dynamic thermal behaviour

(transient thermal impedance) of power electronic devices or converters.

Their purpose is to forecast both the average and fluctuating temperature

profiles that occur during operation. Most of the thermal modelling

techniques are based on reactance theorems defined by Foster and Cauer.

(Foster, 1924; Cauer, 1926). Foster (1924) further improved the model base

approach with adding thermal RC elements. These models offer a high

accuracy as they are executed on a small part of the material in a scaled

system. At the present, Currently, performing transient thermal simulations

for power electronic applications requires significant time and

computational resources. One approach to mitigate this problem is taking

advantage of Fourier in order to avoid the extraction of RC thermal

equivalent circuit. (Culham et al., 2000).
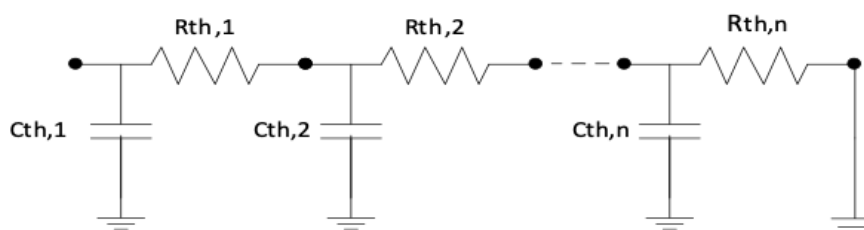
Figure 2-8. Cauer network equivalent thermal circuit

Figure 2.8 demonstrates the equivalent thermal circuit for the Cauer

Network. The advantage of this model is describing the temperature

distribution between the layers in a power semiconductor. Each of the RC networks represent the thermal resistance and capacitance between each layer. The equivalent thermal impedance for Foster Network can be calculated using the below formula:

$$Z_{th}(s) = \cfrac{1}{sC_{th,1} + \cfrac{1}{R_{th,1} + \cfrac{1}{sC_{th,2} + \cfrac{1}{R_{th,2} + \cfrac{1}{\ddots \atop sC_{th,n} + \cfrac{1}{R_{th,n}}}}}}}$$

(2)
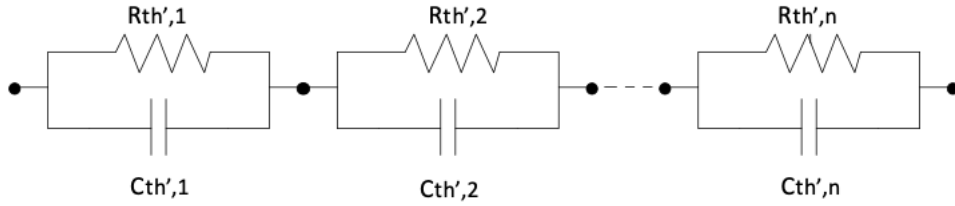
Figure 2-9 Foster Network equivalent thermal model

For each component, the transient thermal impedance is represented by the below formula:

$$\frac{1}{Z_{th}{'}(s)} = \frac{1}{R_{th}{'}} + \frac{1}{sC_{th}{'}} \quad \therefore Z'_{th}(s) = \frac{R'_{th}}{sR'_{th}C'_{th} + 1} = \frac{\frac{1}{C'_{th}}}{s + \frac{1}{\tau}}(3)$$

Where: $\tau = R_{th}C_{th}$ (4)

The thermal impedance information for the power semiconductors is provided in datasheets based on Foster Network. It is possible to convert the

Foster model to Cauer model as demonstrated by Schweitzer et al. (2007) and Gerstenmaier et al. (2007). As established by Musallam et al. (2011), This approach is unable to accurately determine the exact dimensions of the layers because the thermal information provided is purely a mathematical approximation and lacks physical significance. Batunlu (2016) derived a new conversion algorithm from the nth order Cauer to Foster model to overcome this problem.

2.4.2 Finite Element Thermal Modelling

One of the first scientists to utilise Finite Element Modelling (FEM) was Robert Courant in 1943 who utilised the Ritz method to calculate approximate solutions to vibration systems. FEM enables convenient modelling of intricate and non-uniform shapes, providing designers with the capability to analyse the impact of crucial factors on the entire structure, both internally and externally. This allows for a comprehensive understanding of potential failure causes and their implications. There is extensive research on the utilisation of FEM in analysing heat transfer in PECs. Bagnoli et al. (1998) utilised the FEM to design an equivalent circuit for thermal impedance using the Cauer Network. This approach was to only calculate the resistance and capacitance for each layer in a power electronic device in one dimension, but it could not represent the heat dissipation path in the device in three dimensions. An improved thermal model was developed by Masana (1996) which extends the concept of constant angle heat spreading by considering the dimensions of the chip and substrate and

adjusting the spreading angle accordingly. This approach provides closed-form expressions that are sufficiently accurate for practical applications. The model has been applied to circular, square, and rectangular geometries, and the results have been compared with solutions based on Bessel and Fourier series. Masana (2001) further developed the previous model. This research presented an innovative approach for dynamically characterising the thermal behaviour of semiconductor packages. It was built upon the variable angle model for multilayer structures and introduces the evaluation of thermal capacitance for each layer simultaneously and within the same volume used for calculating thermal resistance. This ensured coherence in the analysis. As this volume or lump is dependent on system geometry, materials, and boundary conditions, the model incorporated three-dimensional aspects. The resulting thermal resistances and capacitances, represented as pairs for each layer of the structure, are then utilised as input for an electric circuit simulator to predict the transient response of the package. This approach demonstrated good accuracy however, it could not provide an exact solution to the heat transfer equation and characterise the coupling effect.

Augustin and Hauck (2007) presented a novel approach for developing dynamic thermal compact models that are independent of boundary conditions. The process began by describing the component, such as a semiconductor package or printed circuit board, and defining thermal ports using a finite element code at the continuous field level. Utilising order

reduction techniques, a low-order state space model was derived to capture the thermal behaviour of the component. Further matrix manipulations were applied to transform the state space model into a Kirchhoffian network, which provided transfer functions between all thermal ports. The effectiveness of the method was demonstrated using an example from the semiconductor industry, involving a device package mounted on a printed circuit board. By coupling the models, thermal simulations of the system were conducted, leveraging the newly developed boundary condition independent compact model. This method offered great accuracy however the Lagrange polynomials increased the complexity of the simulation. Batunlu and Albarbar (2016) demonstrated the electrothermal performance of the IGBT chip in a boost converter using FEM and confirmed the results by the aid of electrical measurement, thermal cameras and designing a hardware-in-the-loop experiment using dSPACE. This model achieved an accuracy of 97%.

2.4.2 Acoustic Emissions

Acoustic emissions (AE) have been extensively studied during the past six decades, and it is well established that these signals are emitted from the material under stress. AE technology has a wide spectrum of applications in areas such as material research, non-destructive testing and structural condition monitoring. (Karbhari, 2013) AEs are released when there is a spontaneous release of elastically stored energy during micro or macro failures. This leads into the generation of burst-type transient AE signals with

distinguishable starting and ending points in a timescale between ms - μs. There are other sources for the generation of acoustic signals involving rubbing and friction. AE signals are generally measured using piezoelectric, resonant or wide-band sensors and have a frequency range from between 100 kHz – 1 MHz (Sridharan, 2008)

AE-based condition monitoring is currently utilised in various systems such as pumps, bridges and industrial drives to detect failure and plan preventive maintenance. The benefits of AE-based condition monitoring in power electronic devices were unknown until 2014. Karkkainen et al. (2014) experimentally investigated the acoustic behaviour of a power semiconductor, IGBT, used in a half-bridge configuration consisting of two IGBTs and two diodes. Furthermore, the author included an analysis based on propagation delays determining the possible source of the observed AE signal. The author suggested that the power semiconductor in the circuit was the sole source of the emitted AE. Moreover, the author investigated the possibility of error in measurement and whether there is any electromagnetic interference (EMI) affecting the sensor reading. This was performed by the means of placing a packaging film between the lid and the enclosure. The author concluded that there is no EMI affecting AE emitted from the IGBT.

Müller et al. (2016) studied the effect of aging on the AE signals generated during the chip's aging process. A power cycling test bench was used to investigate the fluctuations of AE signals in an IGBT based three-phase

inverter. In this experiment, an AE sensor was mounted on the heatsink attached to the inverter to record the acoustic events and correlate them with the temperature-sensitive electrical parameters such as the collector-emitter voltage of IGBTs. The author confirmed that there is a correlation between AE and the state of health of the power module by correlating the AE signals with the electrical parameters.

Davari et al. (2018) conducted further experiments which indicate a significant correlation between acoustic emission and on-state voltage drop, which is a commonly used indicator of bond wire lift-off. The results were compared with those obtained from another identical module, and the excellent repeatability observed confirms the high potential of this method for practical applications. The author compared the AE signals between 2475 cycles and suggested that the signal envelope is different at the beginning of the experiment compared to the signal envelope after 2475 cycles. The result of this experiment indicates that there is a correlation between the number of cycles and the AE emitted, and AE levels increase when the device reaches the 2475th Cycle.

Kozak and Gordon (2019) conducted a study to capture the AE signals at the switch on/off states. This was achieved by using a WS alfa AE sensor and then they were amplified, digitised and saved to a local PC for further processing. In this study, the Fast Fourier Transform was utilised to convert the time-domain signal to a frequency-domain signal. In this study, it was confirmed

again that the presence of AE signals is due to the switching nature of power electronic transistor, an IGBT in this study.

He et al. (2021) reviewed the role of AE signals in monitoring various subsystems of RECSs and their efficacy in detecting mechanical defects, such as crack growth. Furthermore, it was suggested that AE sensors could also be employed to detect electromagnetic stress and electrochemical reactions. These AE signals can be instrumental in identifying faults in power electronic devices, transmission and transformation systems, and storage systems. However, the application of AE devices for condition monitoring in RECSs faces significant challenges due to low signal-to-noise ratio (SNR), large data volumes, and performance limitations of the AE devices. The author explored different types of sensors in order to measure the level of AE signals, namely, In this study, by measuring AE signal levels, a linear relationship was found between the turn-off current and the low-frequency component of the AE signal. However, no link was found between the high-frequency component of the AE signal and the turn-off current.

2.5 Summary

Within this chapter, an in-depth exploration of various failure modes in Power Electronic Converters (PEC) was undertaken. As previously highlighted, enhancing the reliability of PEC holds the utmost importance in augmenting the efficiency of Renewable Energy Conversion Systems (RECSs) and positioning them as the leading global energy providers. Over the past two decades, extensive research efforts have been dedicated to advancing

the reliability of PECs, resulting in significant improvements. However, there still exists room for further enhancements in this domain. Notably, this chapter delved into the primary failure modes encountered by Integrated Gate Bipolar Transistor (IGBT) chips, particularly focusing on packaging-related failures stemming from thermomechanical fatigue experienced by the packaging material.

There are multiple methods for controlling the condition of a PEC in a wind turbine in the industry. For instance, monitoring gate-emitter voltage (V_{GE}), collector-emitter saturation voltage ($V_{CE(sat)}$) and internal thermal resistance (R_{th}) are the current parameters to monitor the degradation of the IGBT chip. Moreover, certain operational parameters such as terminal voltages, currents, and ambient and coolant temperatures, among others, are monitored for power electronic converters. The detection of faults in a power converter primarily relies on comparing the reference values with the actual measured values of these parameters or employing model-based techniques. (Wang and Guo, 2007; Karimi et al., 2008; Freire and Cardoso, 2014). The CM based on system parameters has reduced the number of failures in PECs significantly; however, Nevertheless, the utilisation of these signals and techniques for fault localisation and identification of failure modes poses challenges, as distinct failure modes can result in similar patterns in the signals and model outputs.

Acoustic emission-based condition monitoring is a robust, non-intrusive and reliable technique. The only source of acoustic emissions in a power

electronic converter is the power semiconductor and as a result, there is no interference in the monitored signal. Acoustic emission-based condition monitoring is remote. There is no need to access the PEC to measure the signal level. Once the sensor is mounted to the unit, the data can be transmitted to the control centre using SCADA as soon as the AE signal level deviates from the values defined for them.

Chapter 3 : Analysis of Thermal Characteristics of Power Electronic Devices

3.1 Introduction

This chapter delves into the study of heat transfer physics, focusing on the three fundamental modes of heat transfer. Additionally, a thermal model of an IGBT chip is introduced to investigate the heat fluctuations within the chip under specific operating parameters, which are also applied in the experimental section of this research. The objective of this research segment is to illustrate the temperature changes occurring in the power semiconductor chip under particular loading conditions.

3.2 Heat Transfer

Heat transfer refers to the exchange of energy resulting from a difference in temperature within a medium or between multiple mediums. Unlike other forms of energy, heat cannot be stored and is characterised as energy in motion that occurs as a result of temperature differences. (Ghoshdastidar, 2012) The aim of studying heat transfer is to identify the mechanism of it and understand the rate at which the heat is transferred between materials. There are essentially three primary mechanisms of heat transfer, which are conduction, convection, and radiation.

3.2.1 Conduction

Heat conduction is the process of energy transfer within a substance due to molecular motion. When there is a temperature difference between two regions of a body, energy is transmitted from the higher temperature region to the lower temperature region. This energy transfer through molecular

vibrations is known as conduction. (Ghoshdastidar, 2012) Fourier's law

provides the equation for the rate of conduction between two materials:

$$q = -kA(\frac{\delta T}{\delta x}) \qquad (3.1)$$

Where:

q: Rate of Heat Flow

k: Thermal Conductivity (W/mK)

$\frac{\delta T}{\delta x}$: Temperature Gradient (K/m)

A: Area (m^2)

3.2.2 Convection:

Convection refers to the transfer of thermal energy between a solid surface

and a flowing fluid. It is important to note that convection is not considered

as an independent mode of heat transfer. Instead, it signifies a fluid system

in motion, where heat transfer primarily takes place through conduction.

While accounting for the movement of the fluid system in the energy balance

equation, it is crucial to understand that no new fundamental mechanism of

heat transfer is introduced. Newton's law of cooling describes the rate of

convection:

$$q_c = hA(T_S - T_\infty) \qquad (3.2)$$

Where:

h: Heat Transfer Coefficient (W/m^2K)

A: Area (m^2)

T_S: Temperature of the solid (K)

T_∞: Temperature of the Fluid (K)

3.2.3 Radiation

Radiation is a unique form of heat transfer that differs from conduction and convection. It involves the propagation of electromagnetic radiation due to temperature disparities between the bodies involved in heat exchange. This specific type of radiation, resulting from thermal differences, is commonly referred to as thermal radiation. Stefan-Boltzmann law defines the emission of radiations from a black surface:

$$q_{emitted} = \varepsilon \sigma A n^2 T^4 \qquad (3.3)$$

Where:

σ: Stefan-Boltzmann constant ($5.669 \times 10^{-8} \ W/m^2 K^4$)

A: Area (m^2)

n: refractive index of the bounding medium

T: Temperature (K)

ε: emissivity of the surface

Subsequently, the radiation heat loss from a hot surface to a surface with a lower temperature is given by:

$$q_r = \sigma \varepsilon A (T_S^4 - T_\infty^4) \qquad (3.4)$$

Where:

T_S: Temperature of cold surface

T_∞: Temperature of hot surface

Accurate thermal design of semiconductor power electronic devices requires precise determination of the thermal properties of each layer impacted by heat flux. To describe the distribution of heat flux within a material based on its position and properties, the heat diffusion equation is commonly employed. This equation provides a solution for the time-dependent temperature variations within a specified region caused by conduction heat transfer.

$$\frac{\delta^2 T}{\delta x^2} + \frac{\delta^2 T}{\delta y^2} + \frac{\delta^2 T}{\delta z^2} + \frac{q}{k} = \frac{\rho c}{k}\frac{\delta T}{\delta t} \qquad (3.5)$$

Where:

T: Temperature (K)

k: Thermal Conductivity (W/mK)

c: Specific Heat Capacity (J/kgK)

ρ: mass density (kg/m^3)

By taking the Laplace transform of equation 3.5, the heat distribution within the power module can be solved:

$$D(\frac{\delta^2 T}{\delta x^2} + \frac{\delta^2 T}{\delta y^2} + \frac{\delta^2 T}{\delta z^2} = sT - T_0 \qquad (3.6)$$

Where:

D: Diffusion Coefficient

T: Laplace Transform of Temperature

T_0: Initial Temperature

The thermal resistance and thermal capacitance are calculated using the below equations:

$$R_{th} = \frac{l}{kA} \qquad (3.7)$$

Where:

l: Length of the Heated Path (m)

A: Area of the Heated Path m^2

$$C_{th} = c\rho Al \qquad (3.8)$$

3.3 Thermal Resistance

Thermal resistance is a measure of the resistance encountered by heat conduction. It is defined as the ratio of the temperature difference between two specific points to the heat flow between those points over a given period of time. Consequently, higher thermal resistance indicates a greater difficulty in heat conduction, whereas lower thermal resistance implies easier heat conduction.

Figure 3-1. Demonstration of Heat Flow and calculation of thermal resistance

$$R_{th} = \frac{T_1 - T_2}{P} \qquad (3.9)$$

It enables the estimation of the junction temperature (T$_j$) of a semiconductor device when subjected to an input heat source of variable nature, such as PWM.

As discussed in Chapters 1 and 2, IGBTs or power semiconductors in general, are consisted of different layers. These layers are formed of different materials with unique material properties. This difference in material properties leads to a difference in the CTE. When these materials are subjected to a source of heat, they change form differently, which is one of the causes for the packaging-related failure modes in power semiconductors.

3.4 Power Loss Model

In thermal analysis, the crucial input parameter is the power loss. Power loss in Si chips can be categorised into two types: conduction loss and switching loss. These losses can be estimated using either experimental measurements or loss parameters provided in datasheets. Since the primary objective of this chapter is to perform preliminary thermal analysis rather than developing a precise loss model, the power dissipation can be calculated using the datasheet information in this research. The conduction loss in an IGBT is dependent on power factor, drain current etc. The switching current can be calculated by multiplying the turn-on and turn-off energy by the switching frequency.

$$P_{cond} = \left(\frac{1}{2\pi} + \frac{m \times pf}{3\pi}\right) V_{CE} I_{load} + \left(\frac{1}{8} + \frac{m \times pf}{3\pi}\right) R_{dson} I_{load}^2 \quad (3.10)$$

Where:

P_{cond}: IGBT Conduction Losses

pf: Power Factor

V_{CE}: IGBT Collector-Emitter Voltage Drop

R_{dson}: On-Resistance of IGBT

I_{load}: Load Current

$$P_{SW} = \left(E_{on} + E_{off}\right)f_{sw} \qquad (3.11)$$

Where:

P_{SW}: IGBT Switching Loss

E_{on}: IGBT turn-on Energy

E_{off}: IGBT turn-off Energy

f_{sw}: Switching frequency

$$P_{loss} = P_{sw} + P_{cond} \qquad (3.12)$$

3.5 IGBT Internal Structure

After determining the overall power outage, this value can be provided as input for the thermal model. Following that, the thermal model requires the incorporation of material characteristics. As previously mentioned, an IGBT chip is composed of various internal layers, each constructed from different materials possessing distinct properties. Density (ρ), specific heat capacity (c_p) and thermal conductivity are the three parameters required for the thermal model. As discussed earlier, the main factor causing packaging-related failures is the difference in CTE in different materials in the chip and packaging. The temperature fluctuations cause these layers to deform in different ways, leading to failure mechanisms such as solder fatigue and

bond wire lift-off. In order to simulate the heat transfer in an IGBT chip, the three-dimensional geometry is input to the COMSOL Multiphysics Suite. This geometry is demonstrated in Figure 3.2. The next step is to calculate the power losses across the IGBT using equations 3.10 – 3.12 and input this into the model.
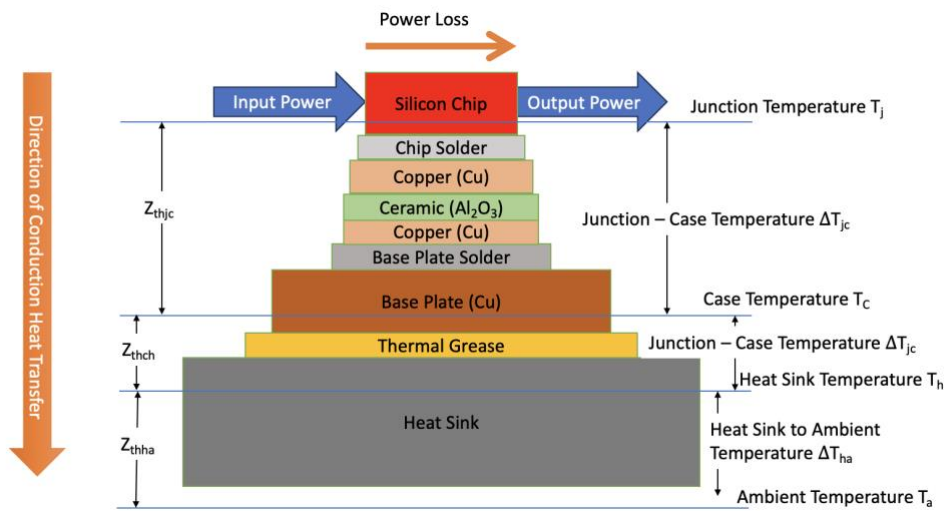
Figure 3-2. Internal structure of an IGBT chip

The power module is distinguished by the bonding of chips (IGBTs) to conductors on an insulating dielectric using solder. The dielectric serves as a medium for heat conduction from the chips and is subsequently soldered to a metal base plate, facilitating the flow of heat to the external heat sink. The use of a heat sink is illustrated in Figure 3.2. However, since this research aims to measure acoustic emissions in elevated temperatures, a heat sink is not used in the FEM model and the boost converter circuit. The use of a heat sink is demonstrated above only to show the placement of this layer with the IGBT chip and packaging.

Layer	Material	Density ρ (kg.m^{-3})	Specific Heat Capacity c_p (J.kg^{-1}.K^{-1})	Thermal Conductivity k (W.m^{-1}.K^{-1})
IGBT Chip	Si	2330	700	130
Chip Solder	60Sn − 40Pb	9000	150	50
DBC Substrate	Cu	8850	385	400
	Al$_2$O$_3$	3900	900	27
	Cu	8700	385	400
Substrate Solder	60Sn − 40Pb	9000	150	50
Baseplate	Cu	8700	385	400

Table 5 Properties and dimensions of materials used in the IGBT chip and packaging.

Figure 3.3 provides a comprehensive outline of the essential stages involved in designing the Finite Element Model (FEM) for an IGBT chip in COMSOL. Initially, the electrical model is created by utilising the datasheet and power loss equations (3.10 – 3.12) to calculate the power loss, denoted as Ploss. This power loss value is subsequently incorporated into the thermal model. To design the FEM, the geometry is defined, and the corresponding material properties are assigned to the model. The diffusion equation (3.6) is employed to solve this particular model.

3.6 IGBT Finite Element Model
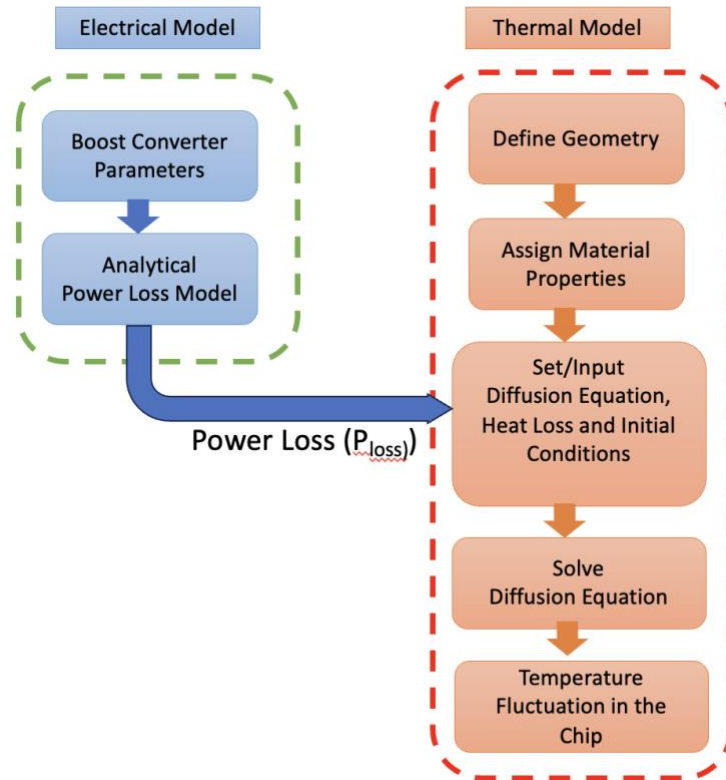
Figure 3-3. IGBT Final Element Model Flowchart
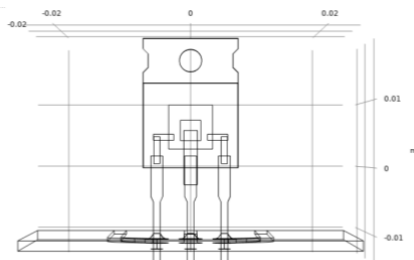
Figure 3-4. View of the IGBT Meshed Model   *Figure 3-5 View of the IGBT Model in*
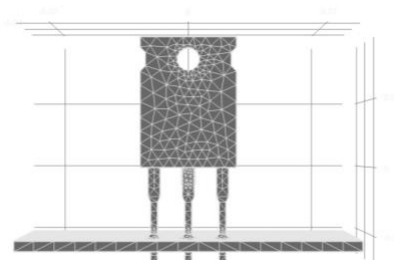
COMSOL

Figure 3.4 and 3.5 illustrate the CAD design that is imported into COMSOL,

as well as the mesh employed in the model. Once the power loss value is

provided as input, the thermal Finite Element Model (FEM) of the IGBT chip

is simulated. Figure 3.6 highlights the regions of heat dissipation and how the heat travels across the chip.
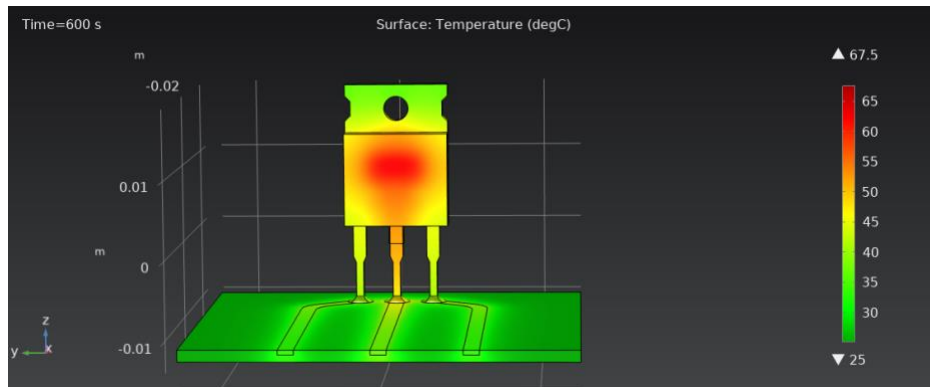
Figure 3-6. Finite Element Model of IGBT demonstrating the Areas of Maximum Heat

In this model, the ambient temperature is set at 20°C, and the model is subjected to a loading condition, simulated for a duration of 800 seconds. The temperature within the chip varies between 30°C and 50°C. As depicted in Figure 3.6, the region surrounding the collector pin exhibits the highest heat accumulation. In this particular model, the collector pin is connected to the IGBT chip whereas the the emitter and gate pins are connected to the wire bond.

Figure 3.7 demonstrates the change in the junction temperature over the period of 800 seconds. As depicted in the figure, the temperature does not exhibit a linear increase. Instead, there is a steep incline between 20°C and 50°C, followed by a gradual rise until the chip temperature reaches its normal operating temperature of 55°C. The subsequent phase of this research involves monitoring the temperature of the IGBT chip within a boost converter circuit and verifying if the temperature variations observed in the experiment align with the outcomes obtained from the Finite Element Model

(FEM). To measure the temperature on the IGBT chip in the boost converter circuit, a thermal camera is employed. This enables confirmation of whether the areas of heat dissipation and high temperatures correspond to the FEM model generated in the preceding chapter.
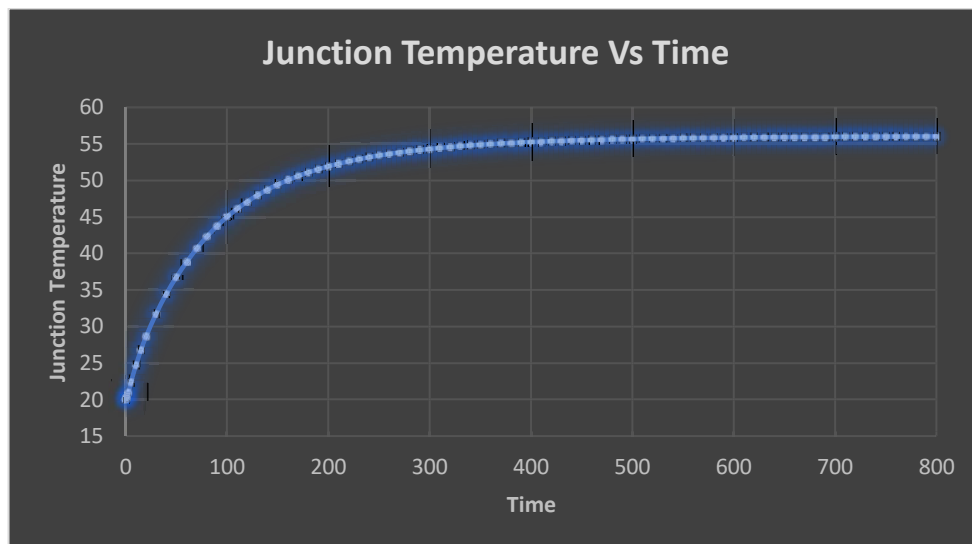
Figure 3-7. Changes in junction temperature over a period of 800 seconds

3.7 Summary

This chapter focused on the analysis of the fundamental structure of IGBTs, highlighting their composition consisting of distinct internal layers, each possessing unique properties. It was emphasised that the variation in material properties within these layers contributes to package-related failures in power semiconductors. The materials, exhibiting different coefficients of thermal expansion, react differently to heat, resulting in diverse deformation patterns and ultimately leading to the formation and propagation of cracks.

This highlights the importance of having efficient means of measuring and monitoring the thermal characteristics of IGBTs or in general power semiconductors. There are various methods of monitoring and modelling the thermal behaviour of these chips which was extensively discussed in Chapter 2. In this experiment, a FEM was designed in order to demonstrate the thermal behaviour of the IGBT chip under certain loading conditions. The same model can be employed to simulate various types of power semiconductors by adjusting the geometry, material properties, and power loss parameters. In this simulation, the focus was on investigating the heat transfer between different layers of the IGBT. It was observed that, under the specific loading condition applied, the temperature increases from the ambient temperature of 20°C to a maximum of 50°C. These findings will be validated through an experiment involving the application of the same loading condition to the IGBT chip within a boost converter. The subsequent objective of this research is to measure the fluctuations in acoustic emission signals emitted by the IGBT chip in a PEC and establish a correlation between these variations and the thermal behaviour of the IGBT.

Chapter 4 : Acoustic Emissions

4.1 Introduction

In Chapter 3, IGBT's Finite Element Model (FEM) and analysed temperature fluctuations during its operation were designed and investigated. The results demonstrated that, under specific loading conditions, the IGBT's temperature increases from the ambient temperature of 20°C to a maximum of 55°C. While extensive research has been conducted to understand the electrothermal and thermomechanical characteristics of power semiconductors, the connection between changes in acoustic emissions and temperature rise remains unclear.

In this chapter, a boost converter is designed, and the data acquisition systems for capturing acoustic emissions are discussed. Various types of AE sensors are examined, leading to the selection of the optimal sensor for recording AE (Acoustic Emission) signals emitted from the boost converter. Ultimately, the chapter aims to compare the level of acoustic signals with the chip's temperature to investigate how the increase in temperature affects the emission of acoustic signals from the IGBT chip.

4.2 Boost Converter Design

In this experiment, a boost converter is used. Boost converters are also known as step-up converters, as the output voltage value is greater than the input voltage. To design a boost converter, the first stage is determining the following parameters.

- Input voltage range ($V_{IN(min)} - V_{IN(max)}$)
- Desired output voltage

- Maximum output current

As well as the above, it's required to select the power semiconductor, IGBT in this case, before the calculations as some parameters are required from the chip datasheet.

The first stage is to calculate the duty cycle. The duty cycle is the ratio of the pulse width to the pulse period. In simpler terms, it demonstrated the fraction of time that the pulse is on in one pulse period. Equation 4.1 is used to calculate the duty cycle of the PWM signal.

$$D = 1 - \frac{V_{IN(\text{min})} \times \eta}{V_{out}}$$ (4.1)

Where:

$V_{IN(min)}$: Minimum input voltage (V)

V_{OUT}: Output voltage

η: Efficiency ≈ 0.8

The next stage in the design of a boost converter is to calculate the ripple current. For most power semiconductors, a range of inductors are specified in the datasheet to be used with the chip. If not specified in the datasheet, Equation 4.3 is used to determine the best inductance value for the circuit. In order to calculate the inductor, ripple current, Equation 4.2 is used.

$$\Delta I_L = \frac{V_{IN(min)} \times D}{f_S \times L}$$ (4.2)

Where:

$V_{IN(min)}$: Minimum input voltage (V)

D: Duty cycle

f_s: Switching frequency

L: Selected inductor value

When there is no inductance specified in the datasheet of the IGBT, Equation 4.3 can be used to calculate the right inductance.

$$L = \frac{V_{in} \times (V_{out} - V_{in})}{\Delta I_L \times f_s \times V_{out}}$$ (4.3)

Where:

V_{IN}: Input voltage

V_{OUT}: Output voltage

f_s: Switching frequency of the converter.

$\Delta I_L = 0.3 \times I_{OUT(max)} \times \frac{V_{OUT}}{V_{IN}}$: estimated inductor ripple current

In Equation 4.3, the value of the inductor current cannot be calculated using Equation 4.2 as the inductance is not known. A good estimation for the inductor ripple current is $20 - 40$ percent of the output current.

To minimise losses, a Schottky diode needs to be used in the boost converter circuit. One of the criteria in selection of a diode is to assure the forward current rating is equal to the maximum output current.

$$I_F = I_{OUT(max)}$$ (4.4)

The other parameter that needs to be checked is the power dissipation of the diode, it needs to handle:

$$P_D = I_F \times V_F$$ (4.5)

Where:

I_F: average forward current of the diode

V_F: Forward voltage of the diode

The next stage is to calculate the output capacitor that is required in the

circuit.

$$C_{out} = \frac{I_{OUT(max)} \times D}{f_s \times \Delta V_{OUT}}$$
(4.6)

For this experiment, the selected IGBT is STGP14NC60KD. Table 6

demonstrates the specification of this chip extracted from the datasheet.

Symbol	Parameter	Value	Unit
V_{CES}	Collector-Emitter Voltage	600	V
I_C	Collector Current at T_C =25°C	25	A
	Collector Current at T_C =100°C	14	A
C_{ies}	Input Capacitance	760	pF
C_{oes}	Output Capacitance	86	pF
C_{res}	Reverse Transfer Capacitance	15.5	pF
Q_g	Total Gate Charge	34.4	nC
Q_{ge}	Gate-Emitter Charge	8.1	nC
Q_{gc}	Gate-Collector Charge	16.4	nC
$t_{d(on)}$	Turn-on Delay Time	22.5	ns
t_r	Current Rise Time	8.5	ns
$t_{d(off)}$	Turn-off Delay Time	116	ns
t_f	Current Fall Time	75	ns
E_{on}	Turn-on Switching Losses at T_C =25°C	82	μJ
E_{off}	Turn-off Switching Losses at T_C =25°C	155	μJ
P_{Loss}	Power Loss at T_C =25°C	112	W

Table 6. IGBT specifications from the datasheet

In the boost converter circuit, an iron-core inductor with an inductance of 1

mH is employed. This particular type of inductor is advantageous due to its

high saturation flux density, which enhances its performance at higher

frequencies.

As for the power diodes, a fast recovery diode is utilised. These diodes are chosen for their short recovery time and low leakage current, contributing to an overall improvement in the total efficiency of the circuit.

The input and output capacitors in the boost converter circuit are of the Cylindrical Aluminium Electrolytic type. To control the ripple of input and output voltages within a 2% range for frequencies ranging from 10 to 100 kHz, 82μF capacitors are chosen for both the input and output sections. Figure 4.1 demonstrates the power boost converter designed for this experiment.

Figure 4-1. IGBT-based DC-DC boost converter.

This boost converter is designed to convert an input voltage of 5 V to a range of output voltages of 8-10V, depending on the value of the duty cycle. With a Duty cycle of 50%, the output voltage is recorded to be 8.5V with an output current of 0.5 A. The PWM input signal to the gate driver circuit is a 30kHz signal with a peak-to-peak amplitude of 10V.

Furthermore, a driver circuit is required to amplify the voltage and current of the signal generated by the function generator for rapid switching of the gate of the power semiconductor. Gate drivers are available both as separate or on-chip modules. In this experiment, a discrete driver circuit is used to

amplify the power of the signal generated by the function generator, as seen in Figure 4.2.
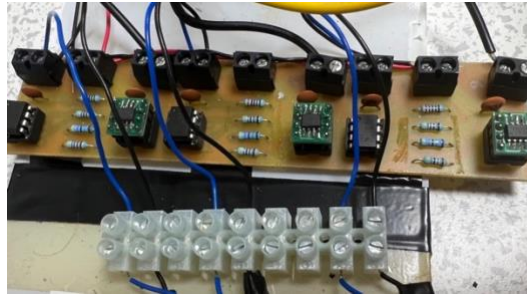
Figure 4-2. IGBT gate driver circuit

4.2 Acoustic Emissions

Acoustic emission (AE) is described as the generation of transient elastic stress waves resulting from the release of energy from a localised source. An AE sensor consists of a thick piezoelectric element that converts the mechanical energy carried by elastic waves into an electrical signal. (Meola and Carlomagno, 2013) Acoustic emissions are a non-destructive evaluation (NDE) technique that detects the high-frequency acoustic energy emitted by an object experiencing stress. Condition monitoring using acoustic emissions have several applications in aerospace, material research and development, transportation and oil and gas. AE signals are mostly utilised to identify crack and crack growth in the material. The benefit of AE-based condition monitoring is not extensively researched in power electronics and detecting a failure in power semiconductors.

In a PEC, the power semiconductor is operated at frequencies ranging from 20 to 50 kHz. Consequently, the device experiences rapid switching on and off up to fifty thousand times per second. This continuous switching action

can be likened to a spring, generating elastic waves. The energy released during these rapid switches contributes to an increase in the temperature of the power semiconductor due to this released energy.

4.3 Measurement of Acoustic Emissions

Acoustic emission testing can be conducted on-site using portable instruments or in a fixed laboratory environment. Typically, the testing systems consist of a sensor, preamplifier, filter, and amplifier, along with measurement, display, and storage equipment such as oscilloscopes, voltmeters, and personal computers. The acoustic emission sensors are designed to detect dynamic motion resulting from an AE event. They achieve this by using transducers that convert mechanical movement into electrical voltage signals. In an AE sensor, the transducer element is typically a piezoelectric crystal, often built from a ceramic material like lead zirconate titanate (PZT). The choice of transducers depends on factors such as the desired operating frequency, sensitivity, and environmental conditions. Ideally, the AE signal received by the data acquisition system should be free of any background noise or electromagnetic interference. The sensors and preamplifiers are specifically designed to minimise and eliminate unwanted signals, thus enhancing the quality of the detected AE signals. Figure 4.3 demonstrates the experimental setup to monitor the acoustic signals emitted from the IGBT chip in a boost converter. Initially, the preamplifier increases the voltage to amplify the signal and enable effective cable transmission. To reduce interference, the preamplifier is positioned near the

sensor. Afterwards, the signal is sent to a bandpass filter, eliminating unwanted frequencies. This filtering is performed in the data acquisition unit based on the threshold defined for the noise levels. Once this filtering is done, the signal is transmitted to a data acquisition system for analysis and storage. Depending on the noise levels, additional filtering or amplification by the preamplifier might still be required.
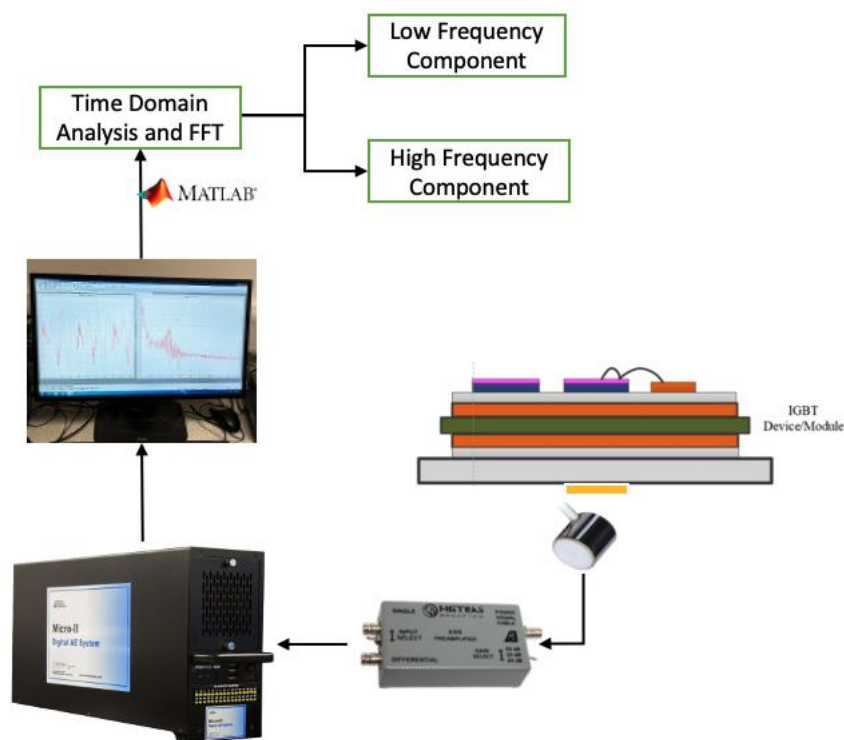
Figure 4-3. Experiment to measure the acoustic emissions from the IGBT

4.3.1 Sensor Selection

The initial step of this experiment involved designing and developing the Boost converter circuit. After completing the design and manufacturing of the boost converter circuit, the next task is to choose an appropriate acoustic emissions sensor to measure the acoustic signals emitted from the IGBT chip

within the boost converter. The selection of the acoustic sensor depends on various factors, such as the frequency range, temperature tolerance, and sensitivity. Several sensors were examined for this experiment to identify the most suitable one that aligns with the requirements of the project. The first sensor tested in this experiment was the R50S general-purpose sensor by the Mistras group. The R50S sensor is a narrowband sensor with high sensitivity, capable of detecting even the smallest acoustic emission signals. It offers an acceptable temperature tolerance ranging from -65℃ to 177℃, with a peak sensitivity of - 62 dB. The operating frequency range for this sensor falls between 100 kHz to 700 kHz. However, the drawback of this sensor is that it cannot detect acoustic emissions in the frequency range of 50 kHz to 100 kHz, nor can it capture any AE activities beyond 700 kHz. Since the objective of this experiment is to identify fluctuations in acoustic emissions across a wide frequency range, using this sensor would have limited the range of frequencies at which acoustic emissions could be studied. Figure 4.4 demonstrates the R50S sensor and the frequency response of this sensor for different frequencies.
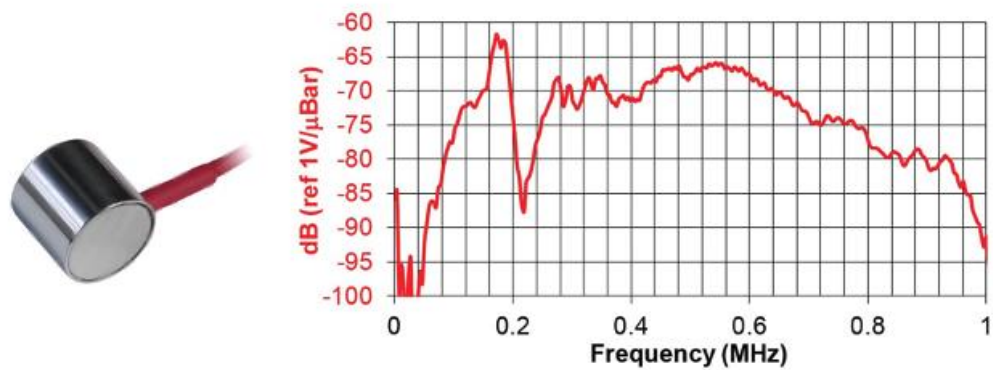
Figure 4-4. R50S narrow-band sensor from Mistras with the corresponding frequency response of the sensor

Another drawback of the R50S sensor is the low sensitivity between 200 – 250kHz frequency range which introduces inaccuracy in the measurements.

After evaluating several options, the WD – 100-900 kHz wideband differential AR sensor was chosen for this experiment. This sensor is a genuine differential wideband sensor with exceptionally high sensitivity and bandwidth. Wideband sensors are particularly well suited for research applications where a high-fidelity AE response is required. Unlike general-purpose sensors, differential sensors employ two sensing elements with opposite polarisations. The two signal leads are fed into a differential preamplifier, effectively eliminating common-mode noise and resulting in lower noise output from the preamplifier. The temperature tolerance of this sensor, ranging from -65°C to 177°C, is comparable to that of the R50S sensor. This indicates that the sensor remains accurate even when exposed to varying temperatures during the experiment.

The WD – 100-900 kHz sensor offers a broader operating frequency range of 125 to 1000 kHz. Additionally, it boasts an almost flat frequency response within this range, ensuring consistent sensitivity throughout this frequency spectrum. Figure 4.5 demonstrates the WD sensor and its frequency response graph.
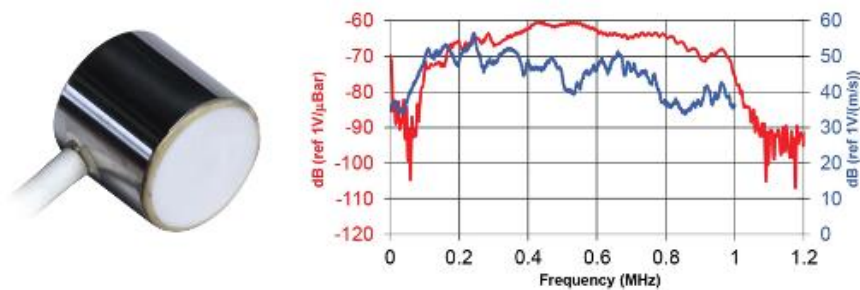
Figure 4-5. WD 100 - 900 kHz wideband differential AE sensor and the corresponding frequency response.

4.3.2 Preamplifier

After evaluating various sensor options for the experiment, it was determined that a voltage preamplifier is required to amplify the voltage output from the chosen sensor. Since the selected sensor is a differential sensor, the preamplifier needs to have a differential input to complement the sensor's functionality. This combination of differential sensor and preamplifier is advantageous as it effectively rejects common-mode noise, leading to a significant reduction in the output noise from the preamplifier. For this experiment, a 2/4/6 preamplifier was selected. This preamplifier provides switch-selectable gain options of 20/40/60 dB. Additionally, the

preamplifier comes equipped with plug-in filters that allow for optimal sensor selectivity and noise rejection. These filters can be configured as low pass, high pass, or band pass, and they offer a constant insertion loss, enabling easy filter swapping without the need for recalibration.

Figure 4-6. A 2/4/6 preamplifier used in the experiment.

As mentioned earlier, the preamplifier offers three different gain settings. For this experiment, the 20 dB gain option was selected. Opting for higher gain settings led to the sensor picking up a significant amount of noise from its surroundings. However, with the 20 dB gain, the sensor only captured acoustic emission (AE) signals when the boost converter circuit was operating. This observation suggests that no electromagnetic interference was present in the data recorded by the sensor.

4.3.3 Data Acquisition

The conventional approach to collecting data from any sensor involves using an analogue-to-digital converter to display the data, typically in voltage form, on an oscilloscope. While this method is accurate, it may introduce inaccuracies when dealing with acoustic emission (AE) signals in the experiment. A custom AE data acquisition system is used for this experiment to ensure minimal data loss.

The chosen data acquisition system is the Micro II – Compact PCI AE Chassis, specifically designed to offer powerful AE testing capabilities in a compact size. It is equipped with 4 PCI-8 AE boards, providing a total of 32 AE channels. The board offers a 10MSPS waveform sampling rate. This kit is designed to function as either a benchtop system directly connected to a monitor, keyboard, and mouse or as a remote system controlled by a laptop through its Ethernet interface. Figure 4.7 demonstrates the PCI-8 system on a board used inside the Micro II data acquisition system.

Figure 4-7. PCI-8, 8-Channel acoustic emission system on a board

Besides its standard PC features, this chassis has specialised features such as integrated AE Hit LEDs. Additionally, it offers audio output capability for AE monitoring through sound feedback. The device has the Physical Acoustics Windows-based AEwin data acquisition and analysis software, which provides features such as 2D and 3D graphing of the collected data, location determination, and the ability to select the filter for each AE channel. Figure 4.8 illustrates the Micro II computer used to capture the data from the AE sensors.

Figure 4-8. Micro II Acoustic Emission data acquisition computer

4.4 Experimental Procedure

So far in this chapter, the emphasis has been on the design of the boost converter used in this experiment. Moreover, a detailed overview of the essential instruments for recording and analysing the acoustic emissions of the boost converter has been presented.

In the experimental part of this research, the boost converter circuit is connected to 5V DC Power Supply. A 30 kHz PWM signal is fed into the gate driver circuit with a peak-to-peak amplitude of 10 V. The duty cycle of the PWM signal is set at 50 percent. The output signal from the gate driver is then connected to the gate of the IGBT to enable the switching of the chip with a frequency of 25 kHz. Furthermore, the output of the boost converter is connected to a load of 10 Ohms. While the circuit is in operation, the temperature of the IGBT chip is measured with a Testo 870 thermal imager. As well as the temperature, the output current and voltage are measured. As shown in Figure 4.9, the boost converter and the driver circuit are powered by two separate power supplies. This setup is necessary because the driver circuit needs an input of 15V, while the boost converter requires 5V. The AE sensor is in contact with the IGBT chip in the boost converter

circuit, separated by a layer of epoxy to prevent any heat transfer from the IGBT chip to the AE sensor. The sensor is then linked to the preamplifier, which is further connected to the Micro II chassis. The display showcases the waveform of the acoustic emissions in both the time and frequency domains.
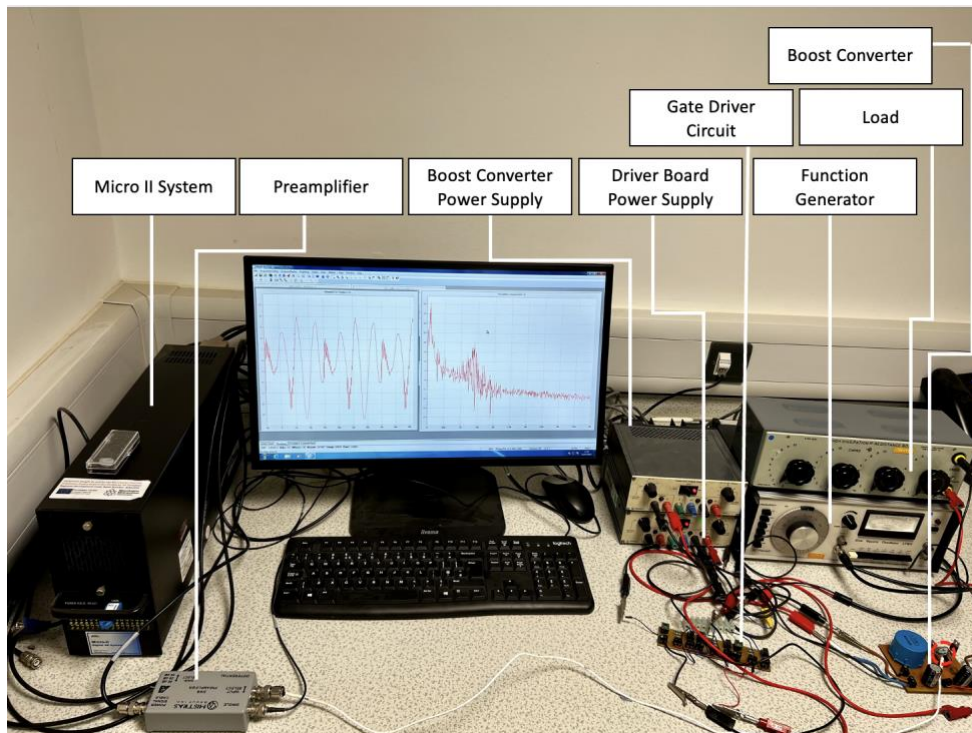
Figure 4-9. Experimental setup for measuring acoustic emissions in a boost converter.

Figure 4.9 provides a detailed view of the AE sensor's placement adjacent to the IGBT chip. There was no need to construct an enclosing module for this experiment, as research by Karkkainen et al. (2014) demonstrated that no EMI was detected by the AE sensors. This was further substantiated in the current study, which found that the sensor did not record any data before the IGBT chip was activated. Furthermore, a layer of thermal gel, which acts as an insulator, was added between the sensor and the device under test to ensure there is minimum heat transfer between the IGBT chip and the AE sensor.
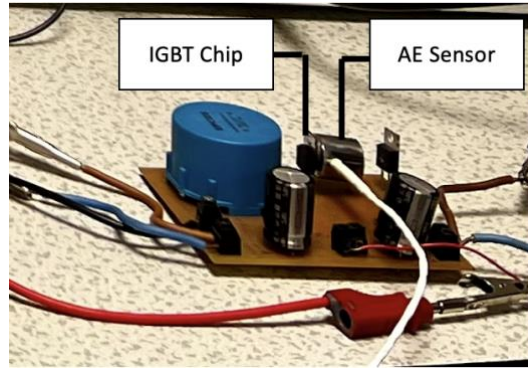
Figure 4-10. AE sensor placement adjacent to the IGBT chip

4.5 Results

In the current experiment, the AE signal produced by the IGBT chip was recorded at every 5℃ rise in the IGBT's temperature. The findings from this experiment are presented in this chapter. Further statistical analysis of these data and an in-depth discussion of the results will be conducted in Chapter 5.
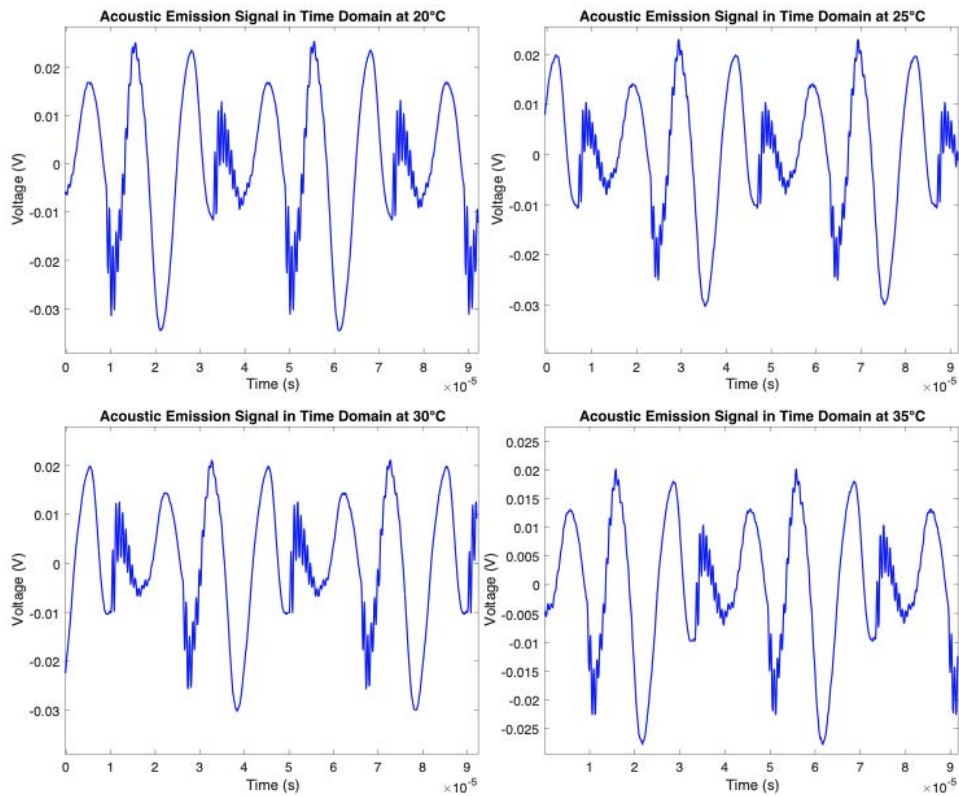
Figure 4-11. Level of acoustic emissions recorded by the sensor for temperatures between 20 -35 ℃
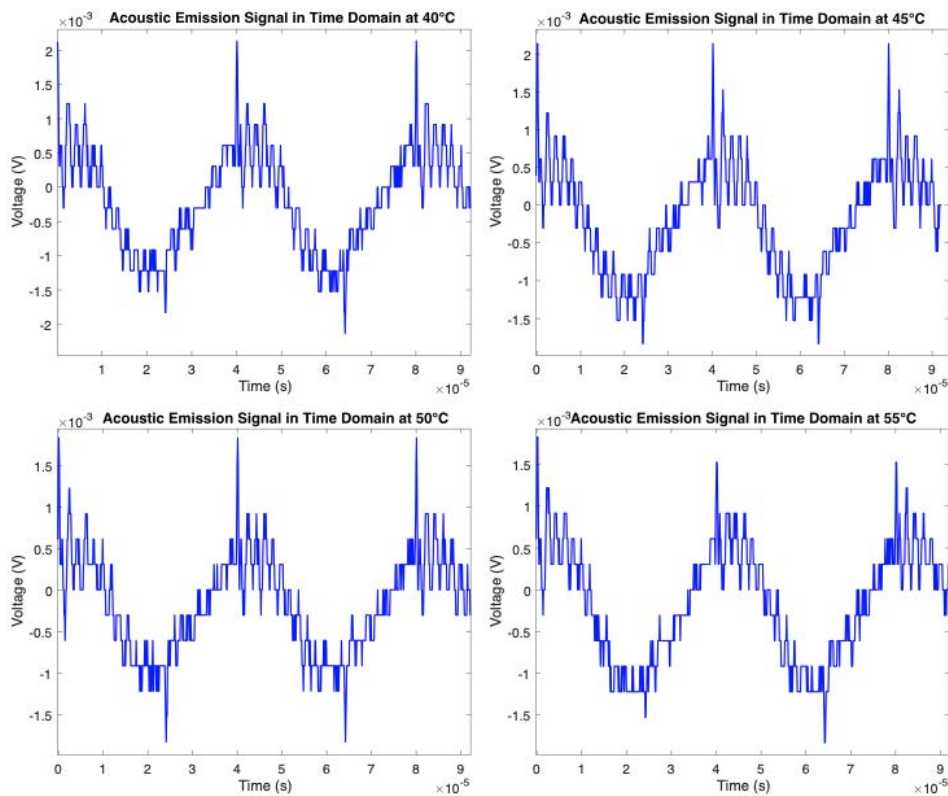
Figure 4-12. Level of acoustic emissions recorded by the sensor for temperatures between 40 -55 ℃

The information derived from the Micro II AE data collection system is showcased in Figures 4.11 and 4.12. What immediately grabs attention in these data points is the noticeable decrease in the AE signal amplitude once the temperature surpasses 35℃. The peak amplitude experiences a substantial reduction from 20 mV down to just 2 mV. This significant decrease in peak amplitude of the detected AE signal can be comprehended through the interplay among stiffness, temperature, and vibrations.

In general, a material's stiffness or modulus of elasticity can change with temperature. For many materials, as temperature increases, they become less stiff. This is because thermal energy allows more movement of the atoms within the material, reducing its resistance to deformation.

Moreover, the stiffness of a material or system is directly related to its vibrational characteristics. According to the theory of vibrations, the natural frequency of vibration of a system is a function of the stiffness of the system and its mass. The stiffer the system, the higher the frequency of vibration. This discussion is in agreement with the above graphs.

As the temperature of the IGBT chip rises, the material softens because the increased thermal energy encourages more particle movement within the chip. This results in a decrease in the amplitude of the detected AE signal. Furthermore, a direct correlation exists between material stiffness and vibration frequency; the stiffer the material, the higher the frequency of its vibrations.

4.6 Summary

In this chapter, Acoustic Emission (AE) technology was explored, emphasising its application in condition monitoring and diagnostics across various fields. We discussed the design of a boost converter using an Insulated Gate Bipolar Transistor (IGBT) with defined input and output voltages and desired output current. This Power Electronic Converter (PEC) is the experimental subject. Additionally, the instrumentation necessary for capturing and measuring AE signals was discussed. In this experiment, the IGBT, functioning as a switching device in the PEC, was determined to be the exclusive source of AE signals. This conclusion was validated by taking AE measurements when the circuit was inactive, indicating that AE signals were only present during PEC

operation, thereby ensuring no electromagnetic interference in the obtained results.

Analysis of the raw data revealed that a temperature rise resulted in a reduction in the peak amplitude of the AE signal, correlating with the relationship between temperature, material stiffness, and vibrations. The findings also indicated that a higher IGBT chip temperature led to a lower signal amplitude across various frequency bands. In the following section, statistical analysis of the AE output signal will be performed to investigate the exact relationship between the chip temperature and the AE signals it emits. This analysis will be primarily based on Fast Fourier transform to identify the signal characterisation in the frequency domain.

Chapter 5 : Results and Discussion

5.1 Introduction

Throughout the course of this doctoral research, we have examined the thermal properties of the IGBT and illustrated the temperature distribution within the IGBT chip. We have recognised the primary regions responsible for heat transfer and have isolated the temperature shifts under particular loading conditions. Additionally, we have extracted the acoustic emissions signals from the boost converter and concluded that an escalation in temperature correlates with a reduction in the AE signal's peak amplitude.

In this chapter, we will undertake a comprehensive statistical analysis to analyse the changes in the frequency domain of the obtained acoustic emission signal concurrent with a temperature rise. In addition to the frequency domain analysis, an examination of the signal in the time domain will also be conducted. This will further elucidate the impact of temperature variations on the acoustic emission (AE) signal within the time domain.

5.2 Time Domain Analysis

The data gathered from the IGBT revealed a notable decrease in the AE signal's amplitude once the temperature crossed the 35 ℃ threshold. In this section, we conduct several analyses on the time domain signal to explore how escalating temperatures influence the AE signal captured within the time domain. Statistical measures such as maximum value, peak-to-peak value, mean and standard deviation were used to find the correlation between the increase in the temperature of the IGBT chip and the level of

acoustic emissions obtained. One of the parameters used is the maximum value of the acoustic signal emitted from the IGBT. The signal has a higher amplitude in lower temperatures and then suddenly after 40℃ it drops significantly.
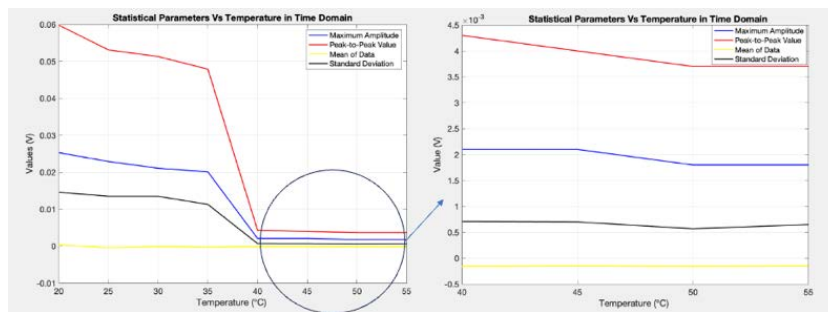
Figure 5-1. Changes in mean, Vpp, standard deviation and maximum amplitude for different temperatures.

Figure 5.1 demonstrates that the maximum AE signal level recorded for the acoustic emissions decreases from approximately 25mV to 2mV when the temperature surpasses 40℃. With the increase in temperature, the material experiences a decrease in stiffness and an increase in damping. Both factors can influence the magnitude of acoustic emissions. An increase in damping reduces the AE signal's amplitude which explains the reason behind the lower amplitude of AE signals at higher temperatures. Furthermore, acoustic emission is a type of testing that involves monitoring ultrasonic waves produced by a material under stress. The speed of sound in solids decreases as temperature increases due to the anharmonic effects of thermal vibrations of the atoms. This can cause a change in the timing or level of the measured acoustic signals, meaning a lower level of acoustic emissions is present at the output of the device. Temperature also influences signal

attenuation. Higher temperatures cause greater signal attenuation, thus reducing the strength of the acoustic emissions.

5.3 Frequency Domain Analysis

In the time domain, a noticeable decline in the signal's peak amplitude was found as the temperature of the IGBT increased. To further probe the properties of the emitted acoustic signals in the frequency domain, it becomes necessary to implement a Fast Fourier Transform (FFT). This process allows the conversion of the time-domain signal into the frequency domain. A frequency domain signal uncovers the range of frequencies inherent in the initial time-domain signal. The magnitude of each peak in the FFT plot symbolises the strength of the corresponding frequency component in the time-domain signal, indicating the intensity of each frequency. One of the essential insights obtainable from the frequency domain analysis is the identification of the dominant signal within the time-domain signal, which is particularly valuable in studying the impact of temperature changes on the AE signals emitted from the power electronic converter.
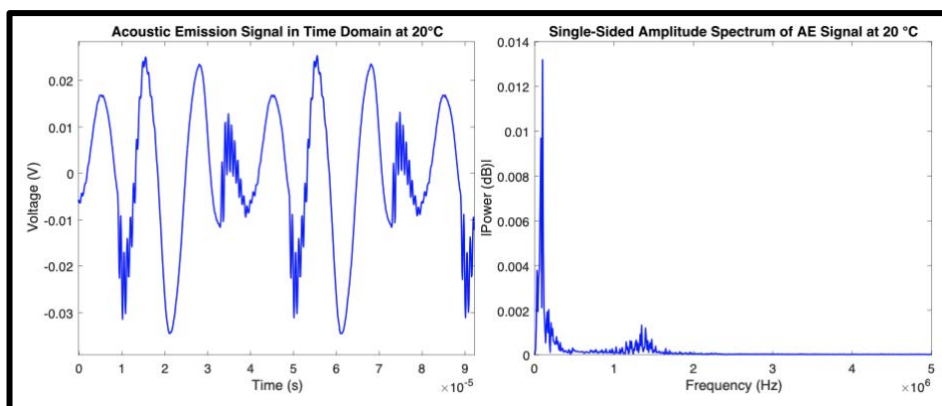
Figure 5-2. Acoustic Emissions in Time Domain (left) and Frequency Domain (right) at 20 ℃
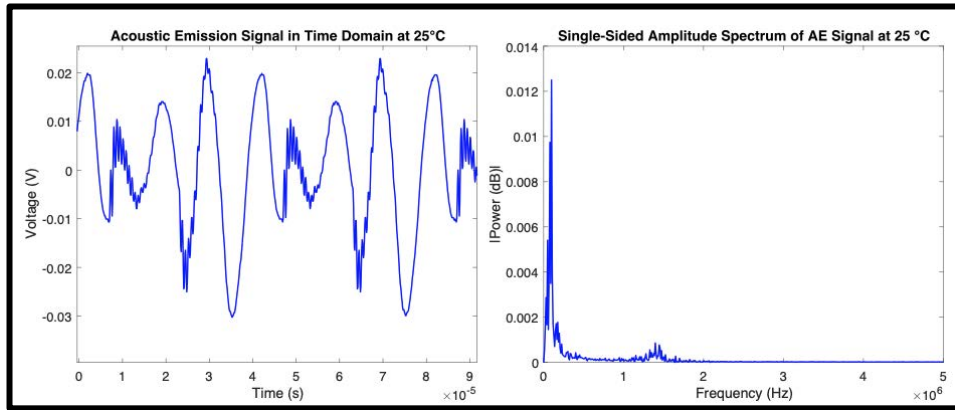
Figure 5-3. Acoustic Emissions in Time Domain (left) and Frequency Domain (right) at 25℃
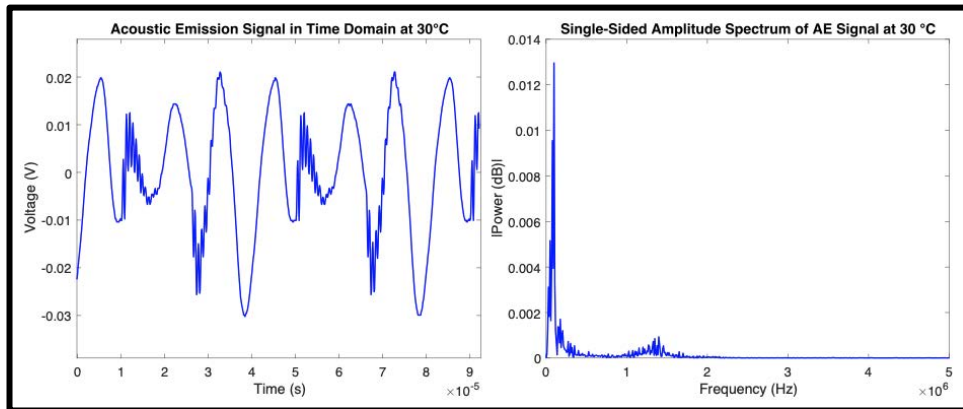
Figure 5-4. Acoustic Emissions in Time Domain (left) and Frequency Domain (right) at 30℃
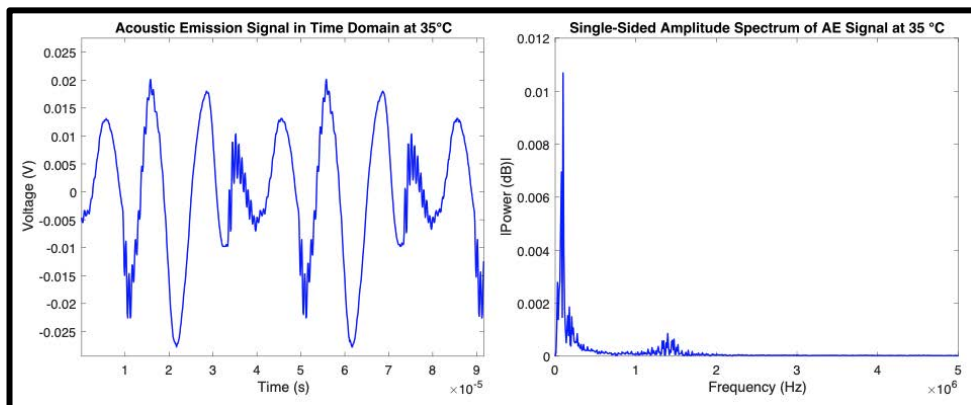
Figure 5-5. Acoustic Emissions in Time Domain (left) and Frequency Domain (right) at 35℃
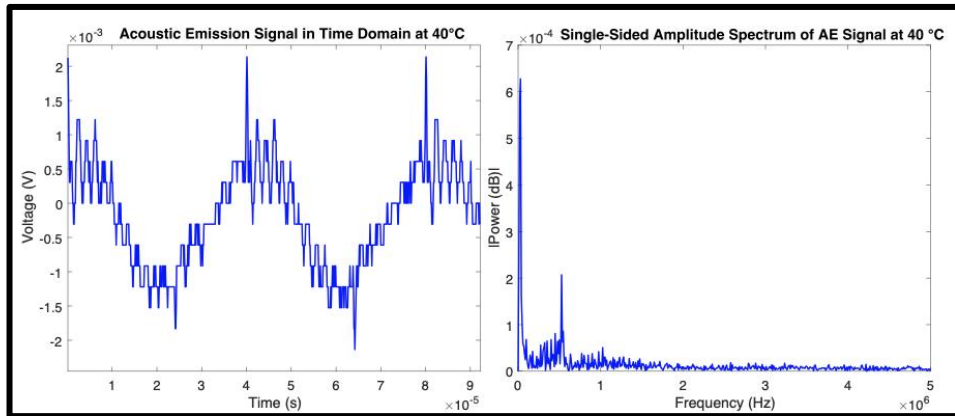
Figure 5-6. Acoustic Emissions in Time Domain (left) and Frequency Domain (right) at 40 ℃
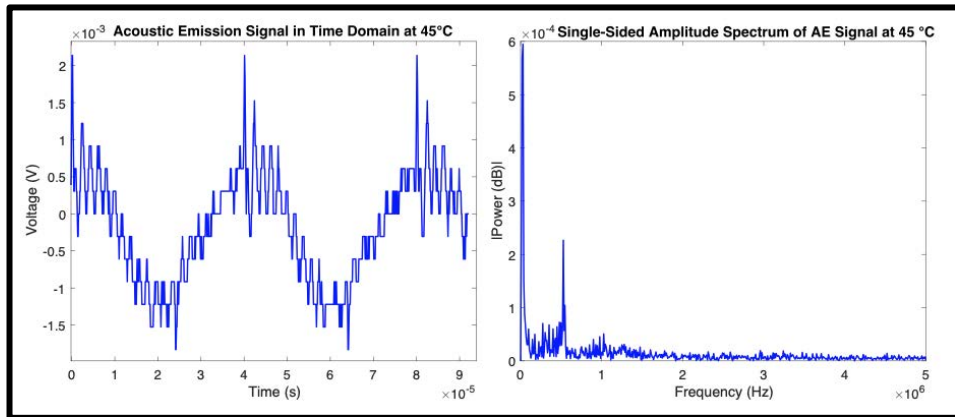
Figure 5-7. Acoustic Emissions in Time Domain (left) and Frequency Domain (right) at 45 ℃
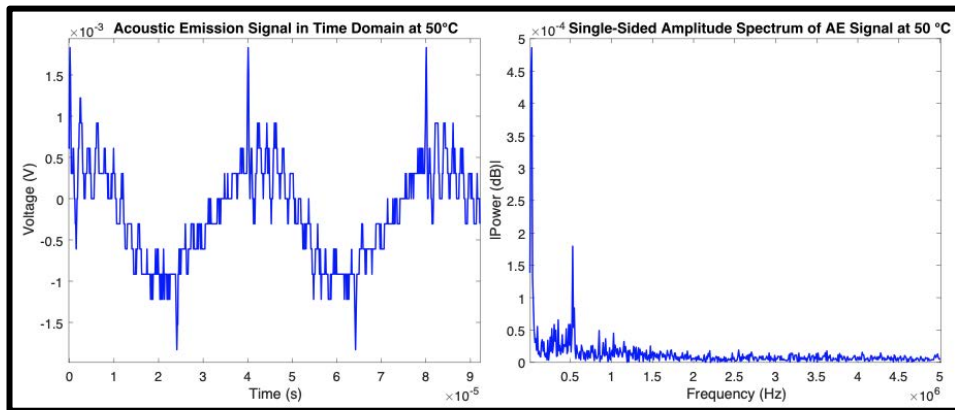
Figure 5-8. Acoustic Emissions in Time Domain (left) and Frequency Domain (right) at 50 ℃
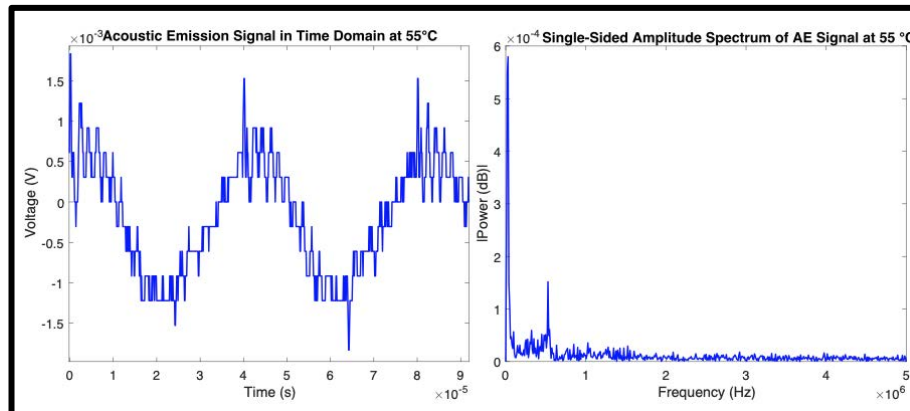
Figure 5-9. Acoustic Emissions in Time Domain (left) and Frequency Domain (right) at 55℃

Figures 5.2-5.9 illustrate the simultaneous time and frequency domains of the Acoustic Emissions (AE) data gathered from the IGBT chip. A noteworthy observation from the single-sided FFT plots is the emergence of new peaks in the frequency range of 400 - 600 kHz with increasing temperature. These peaks start to appear when the temperature surpasses 40℃. Between 40℃ and 55℃, this amplitude slightly decreases from 0.00020 to 0.00015, demonstrating a 25% drop in the peak amplitude of the newly appeared peak in the frequency domain.

5.4 Thermal Imaging

In Chapter 3, a finite element model of the IGBT chip was provided. The FEM highlighted the areas of high heat and given the operating conditions of the circuit designed for the experiment, the model demonstrated an increase in temperature from 20℃ (ambient temperature) to 55℃ over a period of 800 seconds. In the FEM model, the IGBT chip experienced a sharp rise in the temperature up to 40℃, and then gradually the temperature reached 55℃. While performing the acoustic emissions testing, the

temperature of the chip was constantly being measured using an infrared thermal camera. The temperature increment of the IGBT chip is illustrated in Figure 5.10.
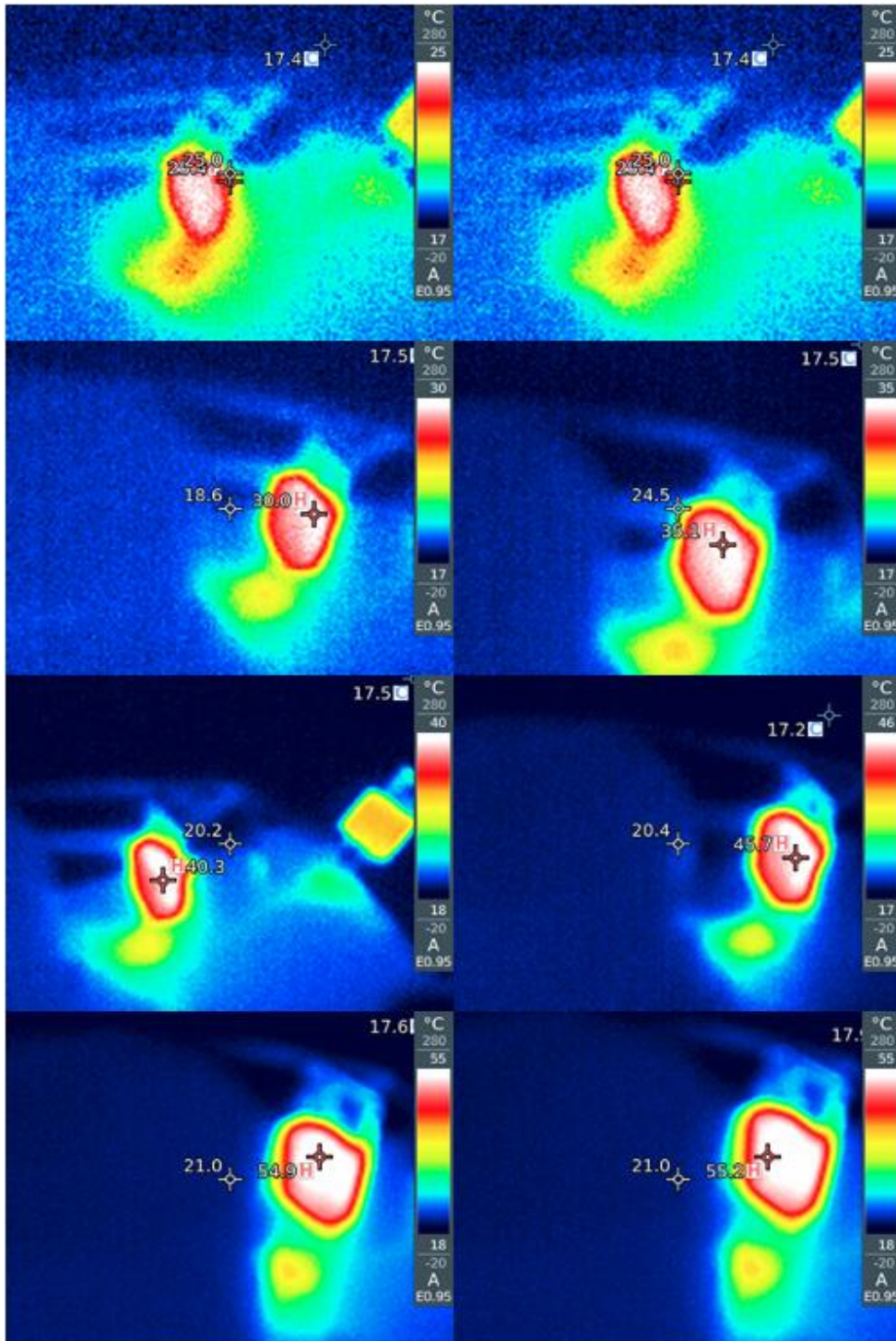
Figure 5-10. Thermal image of the IGBT chip on the boost converter circuit in 5 intervals.

5.5 Discussion

In this experiment, the increase in temperature is carried out under specific operating conditions without the utilisation of accelerated ageing. As a result, the AE signals demonstrated in this research are purely based on the normal operation of the device. The literature available on the measurement of AE is mainly based on accelerated ageing, which in most cases does not demonstrate the natural behaviour of these devices. It is observed in this research that under normal operation of a boost converter, with specific loading conditions, the peak amplitude of the detected AE signal decreases and new peaks appear in the AE signal in the frequency domain. The sudden drop in the peak amplitude of the AE signal and the appearance of these new peaks in the frequency domain indicates that the boost converter is under thermal stress, and it highlights the need for preventive maintenance to avoid failure in the device.

Drawing from existing literature, a rise in temperature typically diminishes the sensitivity of piezoelectric AE sensors. To mitigate potential inaccuracies due to an increase in temperature during the experiment, a layer of thermal gel was used as an insulator between the IGBT chip and the AE sensor, effectively preventing heat transfer from the semiconductor chip to the sensor. Furthermore, the employed sensor in this study has an operational temperature range of -65℃ to 177℃. A behavioural change is observed in the AE signal produced by the IGBT chip as soon as the temperature rises

above 40℃. The alteration in the signal patterns can be understood by examining the physical characteristics intrinsic to acoustic emissions.

Acoustic emissions are the waves of ultrasound and sound that get released when a material undergoes deformation due to various factors. The speed of sound, which affects how quickly AE signals propagate, generally increases as the temperature rises, especially in gases and liquids. This is due to increased molecular activity with higher temperatures, which leads to faster propagation of sound waves.

Moreover, temperature can change a material's physical and mechanical properties, such as its elasticity and thermal expansion. For instance, metals typically expand when heated, which can introduce stresses and change the material's elastic properties. This also has an impact on the generation and propagation of AE signals.

Furthermore, as mentioned earlier, the temperature affects the level of signal attenuation. Signal attenuation means the gradual loss of signal intensity as it propagates through the material. Higher temperatures lead to increased energy dissipation and in turn, increase the attenuation of AE signals.

Chapter 6 : Conclusion and Future Work

6.1 Introduction

This chapter encapsulates the findings of the doctoral research, the core focus of which is an investigation into the thermal and acoustic characteristics of the Insulated Gate Bipolar Transistor (IGBT) chip. This component plays a critical role in power electronic devices utilised in renewable energy conversion systems, such as wind turbines and photovoltaic cells. The study delved into the relationship between changes in thermal attributes and Acoustic Emission (AE) signals emitted from the power semiconductor module during operation within a boost converter. In this section, an overview of the project's objectives is provided, along with a detailed explanation of the methods employed to fulfil them.

6.2 Review of Objectives and Achievements

Objective 1: Gain a clear understanding of the characteristics and working principles of power electronic devices with a focus on those used with renewable energy systems. Namely, boost converters, buck converters, rectifiers and inverters used with solar, wind and fuel cell systems.

Chapters 1 and 2 provided a thorough overview of various PECs utilised in renewable energy conversion systems. Working principles of boost, buck and buck-boost converters were presented. Two-level and multilevel power electronic converter designs were reviewed, highlighting the pros and cons of each configuration. While the choice of topology in PECs can vary based

on the specific application, a consistent feature across all designs is the use of a power semiconductor as the switching device. This research focused on assessing the changes in AE signals with increasing temperature. The outcomes of this study can be extrapolated to various PECs employed in RECSs for system health monitoring purposes.

Objective 2: Literature review of the common failure modes of power electronic devices (PEDs) and currently used monitoring techniques.

In Chapter 2, common modes of failure for PEC were discussed. Two types of failures are associated with power electronic devices, chip-related and packaging-related. These two failure categories can be interconnected when a failure occurs in the power semiconductor. Packaging-related failures arise due to thermomechanical stress and different CTEs between an IGBT's building blocks. By rising temperature, these layers deform in different manners, and this is the main cause of 2 of the most common failure modes, bond-wire lift-off, and solder fatigue. In this chapter, a thorough discussion of currently used condition monitoring techniques in PEC was provided. Furthermore, a comprehensive literature review on using AE signals in predicting failure in power semiconductors was provided. Notably, there exists a gap in the literature concerning the relationship between temperature and changes in AE signals in power semiconductors. This research endeavours to bridge that specific gap.

<u>Objective 3: Develop an Insulated Bipolar Gate Transistor (IGBT) thermal model in COMSOL to understand the effect of thermal stress on the failure modes.</u>

In Chapter 3, an IGBT chip's Finite Element Model (FEM) was developed using COMSOL. The total power loss, determined from the power loss equations using the experimental operational parameters and the chip's datasheet, was fed into this model to pinpoint the IGBT's high-temperature zones and to understand how chip temperature escalates with the provided input. In developing this FEM, specific material properties and dimensions were incorporated to simulate the IGBT chip's thermal dynamics under the given loading conditions. The total power losses in an IGBT is derived from the sum of switching and conduction losses. The results of this simulation were then confirmed with the aid of a thermal camera which confirmed that the changes in temperature of the IGBT over a period is in agreement with the FEM developed.

<u>Objective 4: Verify the outcomes of the developed models through a purposely designed experimental setup. Measurements of temperature and acoustic emissions in addition to power parameters, are expected to be recorded under different operating conditions.</u>

Chapters 4 and 5 demonstrated the experimental procedure for the measurement of AE signals by introducing the instrumentation required to capture the AE signals emitted from the IGBT chip. A boost converter was designed in this experiment, taking an input voltage of 5V and producing an

output of approximately 8V with an output current of 0.5 A with a 10 Ohm load. The IGBT chip was powered by a function generator feeding a PWM signal into the IGBT with a frequency of 25kHz and a peak-to-peak amplitude of 10V.   The AE signals were measured using a piezoelectric sensor which was carefully selected to meet the demands of this research. The selected sensor needed to have a high sensitivity across all frequency bands and offer a suitable temperature tolerance to avoid the adverse effect of high temperature on the sensitivity of the sensor. The AE signal was measured between a temperature range of 20℃ - 55℃. The output signals were analysed in both the time domain and frequency domain to establish the behaviour of AE signals in both domains. In the time domain, the AE data demonstrated an inverse relationship with the chip's temperature, meaning that the peak signal levels dropped in higher temperatures. In the frequency domain, the appearance of new peaks in the range of 400 kHz – 600 kHz was observed.

6.3 Conclusion

This research project successfully met its four primary objectives. The standout and novel contribution of this study was understanding the behaviour of AE signals in relation to temperature increases within an IGBT chip. Initially, the research highlighted the significance of renewable energy systems in addressing the global energy predicament. A major obstacle in transitioning from existing energy sources to renewable ones is the lower efficiency of renewable systems. These renewable systems are intricate,

consisting of multiple subsystems collaborating to convert natural resources into electricity. Over time, each of these subsystems is susceptible to malfunctions. Studying the failure mechanisms and ensuring the reliability of these subsystems is crucial for enhancing their efficiency. To understand the failure mechanisms in these systems, it's essential to study the physics of components and circuits used in these systems.

One of the primary reasons for the malfunction and downtime in renewable energy conversion systems is the failure of power electronic converters. Within PECs, power semiconductors serve as the switching components and often contribute to these failures. Over the years, significant research has been dedicated to pinpointing and understanding the failure modes of PECs. The aim has always been to enhance the design and resilience of these devices, thereby extending their lifespan. As a result, the last two decades have seen considerable improvements in the reliability of both PECs and the broader renewable energy conversion systems they support.

There is extensive literature on the thermal attributes of power semiconductors within PECs, focusing on design enhancements to minimise both electrothermal and thermomechanical stresses. These efforts aim to prolong the operational life of these devices. Such endeavours are facilitated through thermal measurements, modelling, and even assessment of system electrical parameters. In more recent studies, the presence of Acoustic Emissions (AE) near power semiconductors has been explored, revealing that these semiconductors emit AE signals owing to their high-frequency

switching activities. Acoustic emissions are created by the power semiconductor devices as they switch on and off over 20000 times per second, and due to this switching property, the acoustic emissions are released. This research focused on the measurement of acoustic emissions. These acoustic emissions were captured by placing a piezoelectric sensor near the IGBT chip, amplifying the signal using a preamplifier, filtering the noise from the output signal, and finally monitoring the signal on a Micro II AE device. The temperature was recorded using the Testo thermal imaging device, and statistical analysis was performed to understand the changes in the AE signal in both the time domain and frequency domain. It was observed that the peak amplitude of acoustic emissions declined significantly as soon as the temperature surpassed 40℃. Moreover, new peaks appeared in the frequency domain of the signal. Between the temperature of 40℃ - 50℃, the peak amplitude of the newly emerged signal dropped by 25%. Furthermore, it was discussed that the increase in temperature affects the speed of sound and propagation of acoustic waves. Moreover, it was discussed that the increased temperature alters the material properties such as elasticity.

Moreover, the temperature change in the IGBT chip was modelled through a FEM thermal model and confirmed in the experiment. The chip's temperature rose from 20℃ to 55℃, which agrees with the temperatures recorded in the experiment, and the areas of heat transfer are identical to the thermal photos captured during the experiment. The output of this

research can be used to design and implement remote, robust and reliable condition monitoring techniques to alert the site users in case of any abnormalities or sudden drops in the level of AE signals.

The advantage of AE-based condition monitoring systems is the low signal interference, which means no interference from electromagnetic waves. This CM technique is remote, eliminating the need for direct access to the component to measure AE signals. This proves beneficial, especially for offshore wind turbines where site access incurs travel expenses. With a sensor installed close to the circuit, data can be channelled to a computer via SCADA, allowing for real-time monitoring and assessment of the PEC's state of health. AE-based condition monitoring is a non-destructive testing method. This means the data can be collected while the device is operating and there is no need to halt the device to measure the acoustic signals. The benefit of employing this technique over traditional thermal management models is clear. In standard thermal management strategies, heat disperses amongst various components within a power electronic converter (PEC) in a renewable energy conversion system. This dispersion complicates obtaining precise point temperature measurements for the specific device being examined. However, this is not the case for AE signals, as the power semiconductors are the sole components generating AE signals in a PEC. With the correct filtering, the background noise can be removed.

6.4 Future Work

Observing AE signals in PECs is a budding domain with only a handful of literature available. While this research delved into the correlation between escalating temperatures of IGBT chips and AE signals, there remains a significant opportunity to precisely determine the connection between acoustic emissions and the deterioration of PECs. In this research, a small-scale boost converter was used to study the effect of temperature on acoustic emissions. In industry, the PECs consist of multiple power semiconductor elements with higher input voltage and current flow through them. The future work of this research project can be summarised below:

- Integrate an acoustic emissions analysis into the FEM model presented in this research. This would involve modelling AE wave propagation at elevated temperatures, allowing for a simulated examination of how increased temperatures influence acoustic signal levels.

- Measure the acoustic emissions in multilevel large-scale industrial PECs to study the behaviour of acoustic emission signals in PECs.

- Develop a temperature correction algorithm that eliminates heat's effect on the measurement of AE signals to obtain uniform data for different temperature profiles.

- Establish a condition monitoring system that can automatically switch to an alternative PEC within a renewable energy system once the AE signal levels dip below a set threshold. This can be realised by integrating multiple PECs within the renewable energy infrastructure.

As soon as one converter's AE signals fall below the acceptable limits, a backup PEC can be activated, giving the primary converter time to cool down. This approach can significantly minimise wear and tear and reduce the frequency of complete PEC replacements in renewable energy systems.

Appendix I: Mesh Convergence Study

The purpose of this mesh convergence study is to ensure that the results of the IGBT finite element model simulation are independent of the mesh size. This study helps determine the optimal mesh size for the simulation, balancing computational requirements with accuracy.

COMSOL provides various mesh settings for FEMs, ranging from extra coarse to extra fine. To complete this mesh convergence study, the IGBT FEM was simulated with mesh sizes of coarse, normal, fine, and finer to assess the model's accuracy. In the model presented in this research, the normal mesh size was utilised.
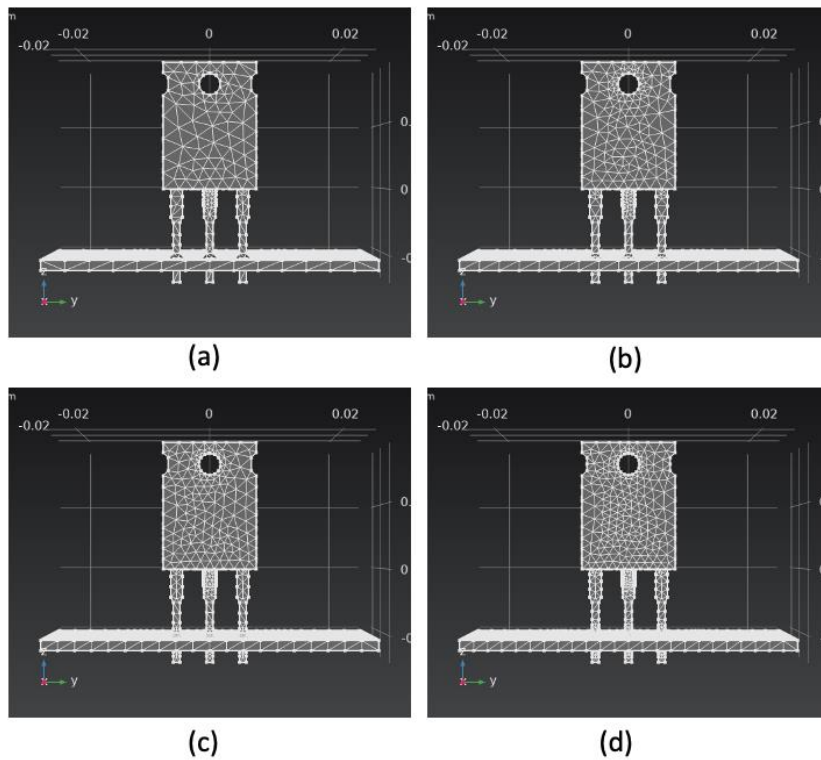
Figure 0-1: Finite element model of IGBT with (a) Coarse Mess (b) Normal Mesh (c) Fine Mesh (d) Finer Mesh

As the mesh size becomes finer, the simulation's accuracy increases. However, using extremely fine meshes requires significantly more computational power. Therefore, in mesh convergence studies, the goal is to compare the model's output with different mesh sizes and establish that the results do not significantly change with further refinements in mesh size.
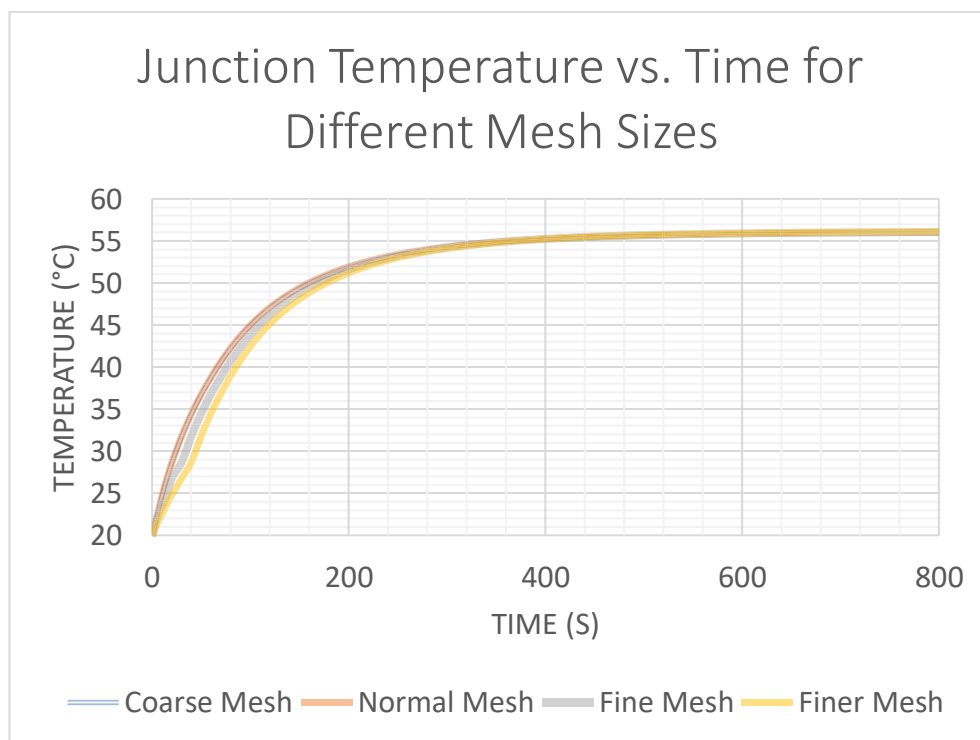
Figure 0-2, Junction temperature versus time for 4 different mesh sizes.

As demonstrated in Figure A-2, there is not a significant difference in the model's output across the various mesh sizes, and they all follow the same pattern. The values for coarse and normal mesh are similar and as a result the coarse mesh is covered by the normal mesh in the above diagram.

To calculate the percentage error in the output of the simulation, based on different mesh sizes, the below equation is used:

$$Percentage\ Error = \left| \frac{T_{j-Normal\ Mesh} - T_{j-Finer\ Mesh}}{T_{j-Finer\ Mesh}} \right| \times 100 \quad \text{(Equation A-1)}$$

For each data point, the absolute difference between the output of the simulation, junction temperature (T_j), is calculated. This difference is then divided by the finer mesh value and multiplied by 100 to convert it to a percentage error. By taking the mean of the percentage errors for all data points, the average percentage difference is calculated to be 2.15%. This consistency suggests that using extremely fine meshes is unnecessary, as the normal mesh provides results comparable to finer mesh sizes. Additionally, simulating this model with extremely fine meshes was not possible due to computational power limitation

Appendix II: Statistical Analysis in MATLAB

In this section, the MATLAB code used to calculate the statistical values for the AE signal is presented. The output AE signal is in the time domain and to transform the acquired data to the frequency domain, fast Fourier transform (FFT) is utilised. Fast Fourier transform is an efficient algorithm to compute the Discrete Fourier Transform (DFT) and its inverse. The formula used to compute the FFT is shown in Equation A-2:

$$X[k] = \sum_{n=0}^{N-1} x[n] \times e^{-j\frac{2\pi}{N}kn}$$
(Equation A-2)

In the above equation, X[k] is the signal in the frequency domain, x[n] is the signal in time domain, N is the number of points in the input signal and $e^{-j\frac{2\pi}{N}kn}$ is the complex exponential function. To calculate the FFT for a time domain signal, as stated by the Nyquist-Shannon sampling theorem, the minimum sampling frequency must be at least twice the maximum frequency component present in the signal. If the signal is sampled below the minimum required sampling frequency, higher frequency components can fold back into the lower frequencies, causing distortion known as aliasing. In this research project, MATLAB is used to calculate the FFT of the AE signal in the time domain to achieve the equivalent signal in frequency domain. This is then plotted in MATLAB for a range of temperatures between

25 -55 °C to study the changes in the frequency domain for the AE signal when the temperature of the IGBT increases.

Furthermore, statistical parameters such as the maximum value, peak-to-peak value, mean, and standard deviation of AE the time-domain signal are calculated to investigate how these values change with increasing temperature in the IGBT chip.

```
clc
clear all
close all

% Time-domain data extracted from the AE acquisition system
%Load data from the csv file
data=load('20deg.csv');
%Extract time and amplitude from the data
Time=data(:,1);
Amp=data(:,2);
%calculate the time step (sampling interval)
dt= Time(2)- Time(1);

%Calculate statistical parameters of the time-domain signal
S=skewness(Amp);
M= mean(Amp)
Max=max(Amp)
st=std(Amp)
pp=max(Amp)-min(Amp)
%Create a matrix of the calculated statistical data
Mat=[M Max st pp];
%plot the AE signal in time-domain
figure(1)
plot(Time,Amp,'LineWidth',1.5,'color','b');
title(['Acoustic Emission Signal in Time Domain at ' ...
```

```matlab
    '55℃'])
xlabel('Time (s)')
ylabel('Voltage (mV)')

% extract the amplitude mean value to normalise it
Amp = Amp - mean(Amp);

%determine the number of data points
n = length(Time);
%calculate the sample rate
SampleRate=1/dt;
L = length(Time);
%determine the next power of 2 from the length of the signal.
NFFT = 2^nextpow2(L); % Next power of 2 from length of y
%Calculate FFT of the AE signal.
Y = fft(Amp,NFFT)/L;
f = SampleRate/2*linspace(0,1,NFFT/2+1);

% Plot single-sided amplitude spectrum.
figure(2)
plot(f,2*abs(Y(1:NFFT/2+1)),'LineWidth',1.5,'color','b')

title(['Single-Sided Amplitude Spectrum of X(t) at ' ...
    '55 ℃'])
xlabel('Frequency (Hz)')
ylabel('|Power (dB)|')
```

References

Alvarez, R., Filsecker, F., Bernet, S. and Ieee. (2011) *Comparison of Press-Pack IGBT at Hard Switching and Clamp Operation for Medium Voltage Converters.* Birmingham, ENGLAND, Aug 30-Sep 01. NEW YORK: Ieee.

Amerasekera, E. and Njim, F. (1997) *Failure Mechanisms in Semiconductor Devices.* Wiley.

Augustin, A. and Hauck, T. (2007) *A New Approach to Boundary Condition Independent Compact Dynamic Thermal Models.* 18-22 March 2007.

Bagnoli, P. E., Casarosa, C., Ciampi, M. and Dallago, E. (1998) 'Thermal resistance analysis by induced transient (TRAIT) method for power electronic devices thermal characterization. I. Fundamentals and theory.' *IEEE Transactions on Power Electronics*, 13(6) pp. 1208-1219.

Baliga, B. (1995) Insulated gate bipolar transistor with reduced susceptibility to parasitic latch-up. In: Patent, U. S. Vol. 5,396,087.

Batunlu, C. (2016) *Thermal characterisation and reliability analysis of power electronic devices in wind and solar energy systems.* PhD. Manchester Metropolitan University.

Batunlu, C. and Albarbar, A. (2016) 'Real-time system for monitoring the electro-thermal behaviour of power electronic devices used in boost converters.' *Microelectronics Reliability*, 62, 2016/07/01/, pp. 82-90.

Blaabjerg, F., Liserre, M. and Ma, K. (2012) 'Power Electronics Converters for Wind Turbine Systems.' *Ieee Transactions on Industry Applications*, 48(2), Mar-Apr, pp. 708-719.

Busca, C., Teodorescu, R., Blaabjerg, F., Munk-Nielsen, S., Helle, L., Abeyasekera, T. and Rodriguez, P. (2011) 'An overview of the reliability prediction related aspects of high power IGBTs in wind power applications.' *Microelectronics Reliability*, 51(9-11), Sep-Nov, pp. 1903-1907.

Carrasco, J. M., Franquelo, L., Bialasiewicz, J., Galvan, E., Portillo, R., Prats, M. M., Leon, J. and Moreno-Alfonso, N. (2006) 'Power-Electronic Systems for the Grid Integration of Renewable Energy Sources: A Survey.' *Industrial Electronics, IEEE Transactions on*, 53, 07/01, pp. 1002-1016.

Castaldo, A. (2012) *Switching regulator fundamentals.* SNVA559C, Texas Instruments.

Cauer, W. (1926) 'Die Verwirklichung der Wechselstromwiderstände vorgeschriebener
Frequenzabhängigkeit.' pp. 355 - 388.

Ciappa, M., Castellazzi, A. and Ieee. (2007) *Reliability of high-power IGBT modules for traction applications.* Phoenix, AZ, Apr 15-19. NEW YORK: Ieee.

Ciprian, R., Lehman, B. and Ieee. (2009) *Modeling Effects of Relative Humidity, Moisture, and Extreme Environmental Conditions on Power Electronic Performance.* San Jose, CA, Sep 20-24. NEW YORK: Ieee.

Culham, J. R., Yovanovich, M. M. and Lemczyk, T. F. (2000) 'Thermal characterization of electronic packages using a three-dimensional Fourier series solution.' *Journal of Electronic Packaging*, 122(3), Sep, pp. 233-239.

Davari, P., Kristensen, O. and Iannuzzo, F. (2018) 'Investigation of acoustic emission as a non-invasive method for detection of power semiconductor aging.' *Microelectronics Reliability*, 88-90, 2018/09/01/, pp. 545-549.

Faulstich, A., Stinke, J. K. and Wittwer, F. (2005) 'Medium voltage converter for permanent magnet wind power generators up to 5 MW.' *Proc. EPE*, pp. 1-9.

Foster, R. M. (1924) 'A Reactance Theorem.' *Bell Systems Technical Journal*, 3 pp. 259 - 267.

Freire, N. M. A. and Cardoso, A. J. M. (2014) 'Fault-Tolerant PMSG Drive With Reduced DC-Link Ratings for Wind Turbine Applications.' *Ieee Journal of Emerging and Selected Topics in Power Electronics*, 2(1), Mar, pp. 26-34.

Ganthia, B. P., Barik, S. K. and Nayak, B. (2021) 'Wind Turbines in Energy Conversion System: Types & Techniques.' *In* Singh, V. K., Bhoi, A. K., Saxena, A., Zobaa, A. F. and Biswal, S. (eds.) *Renewable Energy and Future Power Systems*. Singapore: Springer Singapore, pp. 199-217. [Ganthia2021]
https://doi.org/10.1007/978-981-33-6753-1_9

Gerstenmaier, Y. C., Kiffe, W., Wachutka, G. and Eda. (2007) *Combination of thermal subsystems modeled by rapid circuit transformation.* Budapest, HUNGARY, Sep 17-19. GRENOBLE: Eda Publishing.

Ghoshdastidar, P. S. (2012) 'Heat Transfer.' *In Heat Transfer (2nd Edition)*. Oxford University Press,
https://app.knovel.com/hotlink/pdf/id:kt00TVI4K1/heat-transfer-2nd-edition/applications-heat-transfer

Grant, D. A. and Gowar, J. (1989) *Power MOSFET-Theory and Applications.* Wiley.

Han, Y. and Song, Y. H. (2003) 'Condition monitoring techniques for electrical equipment - A literature survey.' *Ieee Transactions on Power Delivery*, 18(1), Jan, pp. 4-13.

Hansen, A. D. and Hansen, L. H. (2007) 'Wind turbine concept market penetration over 10 years (1995-2004).' *Wind Energy*, 10(1), Jan-Feb, pp. 81-97.

He, Y., Li, M., Meng, Z., Chen, S., Huang, S., Hu, Y. and Zou, X. (2021) 'An overview of acoustic emission inspection and monitoring technology in the key components of renewable energy systems.' *Mechanical Systems and Signal Processing*, 148, 2021/02/01/, p. 107146.

Held, M., Jacob, P., Nicoletti, G., Scacco, P. and Poech, M. H. (1997) *Fast power cycling test for IGBT modules in traction application.* Singapore, Singapore, May 26-29. NEW YORK: I E E E.

Jakob, R., Keller, C., Moehlenkamp, G., Gollentz, B. and Ieee. (2007) *3-level high power converter with press pack IGBT.* Aalborg, DENMARK, Sep 02-05. PISCATAWAY: Ieee Service Ctr.

Kameda, K. (2008) *Motor driving device having MOSFET MOSFET and motor having MOSFET.*

Karbhari, V. M. (2013) '1 - Introduction: the future of non-destructive evaluation (NDE) and structural health monitoring (SHM).' *In* Karbhari, V. M. (ed.) *Non-Destructive Evaluation (NDE) of Polymer Matrix Composites*. Woodhead Publishing, pp. 3-11. https://www.sciencedirect.com/science/article/pii/B9780857093448500014

Karimi, S., Gaillard, A., Poure, P. and Saadate, S. (2008) 'FPGA-Based Real-Time Power Converter Failure Diagnosis for Wind Energy Conversion Systems.' *Ieee Transactions on Industrial Electronics*, 55(12), Dec, pp. 4299-4308.

Karkkainen, T. J., Talvitie, J. P., Kuisma, M., Hannonen, J., Strom, J. P., Mengotti, E. and Silventoinen, P. (2014) 'Acoustic Emission in Power Semiconductor Modules-First Observations.' *Ieee Transactions on Power Electronics*, 29(11), Nov, pp. 6081-6086.

Katsis, D. C. and van Wyk, J. D. (2003) 'Void-induced thermal impedance in power semiconductor modules: Some transient temperature effects.' *Ieee Transactions on Industry Applications*, 39(5), Sep-Oct, pp. 1239-1246.

Kozak, M. and Gordon, R. (2019) 'Experimental investigations of monolithic IGBT transistor acoustic emission phenomena.' *ITM Web Conf.*, 28 p. 01036.

Li, H., Peng, W. W., Huang, C. G. and Soares, C. G. (2022) 'Failure Rate Assessment for Onshore and Floating Offshore Wind Turbines.' *Journal of Marine Science and Engineering*, 10(12), Dec,

Maouad, A., Hoffmann, A., Khoury, A. and Charles, J. P. (2000) 'Characterization of high-density current stressed IGBTs and simulation with an adapted SPICE sub-circuit.' *Microelectronics Reliability*, 40(6), Jun, pp. 973-979.

Masana, F. N. (1996) 'A closed form solution of junction to substrate thermal resistance in semiconductor chips.' *IEEE Transactions on Components, Packaging, and Manufacturing Technology: Part A*, 19(4) pp. 539-545.

Masana, F. N. (2001) 'A new approach to the dynamic thermal modelling of semiconductor packages.' *Microelectronics Reliability*, 41(6), 2001/06/01/, pp. 901-912.

Meola, C. and Carlomagno, G. M. (2013) '14 - Non-destructive evaluation (NDE) of aerospace composites: detecting impact damage.' *In* Karbhari, V. M. (ed.) *Non-Destructive Evaluation (NDE) of Polymer Matrix Composites*. Woodhead Publishing, pp. 367-396.
https://www.sciencedirect.com/science/article/pii/B9780857093448500142

Müller, S., Drechsler, C., Heinkel, U. and Herold, C. (2016) *Acoustic emission for state-of-health determination in power modules.* 21-24 March 2016.

Musallam, M., Johnson, C. M. and Ieee. (2011) *Impact of Different Control Schemes on the Life Consumption of Power Electronic Modules for Variable Speed Wind Turbines.* Birmingham, ENGLAND, Aug 30-Sep 01. NEW YORK: Ieee.

Ohring, M. and Kaszprzak, L. (2014) *Reliability and Failure of Electronic Materials and Devices.*

Patil, N., Das, D., Goebel, K., Pecht, M. and Ieee. (2008) *Identification of Failure Precursor Parameters for Insulated Gate Bipolar Transistors (IGBTs).* Denver, CO, Oct 06-09. NEW YORK: Ieee.

Ratchev, P., Vandevelde, B. and De Wolf, I. (2004) 'Reliability and failure analysis of Sn-Ag-Cu solder interconnections for PSGA packages on Ni/Au surface finish.' *Ieee Transactions on Device and Materials Reliability*, 4(1), Mar, pp. 5-10.

Rodriguez, J., Bernet, S., Steimer, P. K. and Lizama, I. E. (2010) 'A Survey on Neutral-Point-Clamped Inverters.' *Ieee Transactions on Industrial Electronics*, 57(7), Jul, pp. 2219-2230.

Schweitzer, D., Pape, H. and Chen, L. (2007) *Transient measurement of the junction-to-case thermal resistance using structure functions: Chances and limits.* San Jose, CA, Mar 16-20. NEW YORK: Ieee.

Sridharan, S. (2008) 'Index.' *In* Sridharan, S. (ed.) *Delamination Behaviour of Composites*. Woodhead Publishing, pp. 741-762.
https://www.sciencedirect.com/science/article/pii/B9781845692445500304

Strzelecki, R. and Zinoviev, G. S. (2008) 'Overview of Power Electronics Converters and Controls.' *In* Strzelecki, R. M. and Benysek, G. (eds.) *Power Electronics in Smart Electrical Energy Networks*. London: Springer London, pp. 55-105. [Strzelecki2008] https://doi.org/10.1007/978-1-84800-318-7_3

Sze, S. N. (1981) *Physics of Semiconductor Devices.* Wiley.

Teichmann, R. and Bernet, S. (2005) 'A comparison of three-level converters versus two-level converters for low-voltage drives, traction, and utility applications.' *Ieee Transactions on Industry Applications*, 41(3), May-Jun, pp. 855-865.

Tenca, P., Rockhill, A. A., Lipo, T. A. and Tricoli, P. (2008) 'Source topology for wind turbines with decreased mains current harmonics, further reducible via functional minimization.' *Ieee Transactions on Power Electronics*, 23(3), May, pp. 1143-1155.

Thebaud, J. M., Woirgard, E., Zardini, C., Sommer, K. H., Ieee and Ieee. (2000) *Extensive fatigue investigation of solder joints in IGBT high power modules.* Las Vegas, Nv, May 21-24. NEW YORK: Ieee.

Timbus, A., Teodorescu, R., Blaabjerg, F., Liserre, M. and Ieee. (2005) *Synchronization methods for three phase distributed power generation*

systems. An overview and evaluation. Recife, BRAZIL, Jun 12-16. NEW YORK: Ieee.

Valentine, N., Das, D. and Pecht, M. (2015) 'Failure Mechanisms of Insulated Gate Bipolar Transistors (IGBTs).' Presentation at University of Maryland,

Wang, Z. and Guo, Q. (2007) 'The diagnosis method for converter fault of the variable speed wind turbine based on the neural networks.' *In 2nd International Conference on Innovative Computing, Information and Control* pp. 615-615.

Wu, B., Lang, Y., Zargari, N. and Kouro, S. (2005) *Power Conversion and Control of Wind Energy Systems.* Wiley.

Yang, S. Y., Xiang, D. W., Bryant, A., Mawby, P., Ran, L. and Tavner, P. (2010) 'Condition Monitoring for Device Reliability in Power Electronic Converters: A Review.' *Ieee Transactions on Power Electronics*, 25(11), Nov, pp. 2734-2752.